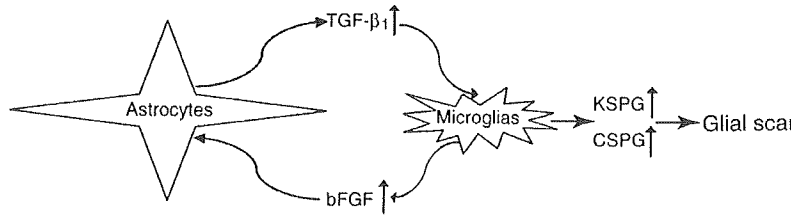

Fig. 7 – Schematic diagram showing the cross talk between astrocytes and microglias. The cross talk is accomplished by TGF-β_1 and bFGF, and results in the production of KS and CS, which leads to the inhibition of neuronal axon regeneration.

conditioned medium from bFGF-treated astrocytes (bFGF-ACM) induced KS and CS expression in primary cultured microglias, and TGF-β_1-neutralizing antibody suppressed the expression. Our data therefore suggest that TGF-β_1 and bFGF establish cross talk between astrocytes and microglias after neuronal injuries (Fig. 7). bFGF and TGF-β_1 induce CS expression in astrocytes and astrocyte migration, which together are sometimes regarded as astrocyte activation, and thus could promote glial scar formation (Faber-Elman et al., 1996). We have demonstrated that bFGF alone can induce CS expression in microglias (Fig. 6). However, the extent of KC and CS induction by bFGF alone in microglias is much smaller than that by bFGF-ACM (Fig. 6). Furthermore, immunohistochemistry demonstrates that a large portion of KS- and CS-positive signals merge with microglias after neuronal injury (Figs. 1, 2). Based on these findings, it is likely that the cross talk between astrocytes and microglias mediated by TGF-β_1 and bFGF plays an indispensable role in inducing KS and CS biosynthesis after injury (Fig. 7).

It has been recently reported that ligands for the EGF receptor (ErbB1), including EGF, TGF-α and HB-EGF, are potent inducers of CSPG production in astrocytes (Smith and Strunz, 2005). A specific inhibitor for ErbB1 suppresses CSPG production by astrocytes after treatment with these ligands. Although TGF-α is consistently expressed, ErbB1 expression is induced by brain injury. Thus, signaling through ErbB1 in astrocytes plays an important role in CSPG production after injury. Smith and Strunz also reported that TGF-β_1 induces CSPG production to some extent (Smith and Strunz, 2005). CSPG production by astrocytes through growth factors or cytokines has also been established in other studies (Asher et al., 2000; Properzi et al., 2005). In this context, our present study has provided an additional notion that KS- and CS-biosynthesis share a regulatory mechanism in common in microglias. Taken together, the common mechanism of KS- and CS-biosynthesis may include activation of both astrocytes and microglias by growth factors, such as TGF-β_1, bFGF and TGF-α.

TGF-β's actions on inflammatory cells after neuronal injury are complex and contextual. TGF-β_1 induces ramification in microglias (Schilling et al., 2001) as well as antioxidant gene expression in microglia *in vitro*, and thus modulates microglial redox status and activation state (Min et al., 2006). Astrocytes appear to suppress microglial production of nitric oxide through a mechanism involving activation of the latent form of TGF-β (Vincent et al., 1997, 1998). Overexpression or injection of TGF-β_1 in the CNS suppresses microglial activation and consequently the induction of the pro-inflammatory chemokines after hypoxic/ischemic injury (Gross et al., 1993; McNeill et al., 1994; Henrich-Noack et al., 1996). In contrast, the overproduction of TGF-β_1 by astrocytes aggravates CNS inflammation (Wyss-Coray et al., 1995), and injection of TGF-β_1-neutralizing antiserum suppresses CNS inflammation after injury (Logan et al., 1999; King et al., 2004). Our present study has shown that bFGF-stimulated astrocytes produce sufficient levels of TGF-β_1 to induce KS and CS expression in microglias. It is noteworthy that raised levels of TGF-β correlate with the deposition of scar materials after traumatic injury to the CNS (Logan et al., 1992). A combination of antibodies to TGF-β_1 and TGF-β_2 reduces scar formation after the nigrostriatal tract is cut (Moon and Fawcett, 2001). Furthermore, mice deficient in smad3, a TGF-β-specific intracellular signaling molecule, display reduced scar formation after a stab wound to the cerebral cortex (Wang et al., 2007). These results suggest that KS and CS production in microglias via TGF-β_1 contributes to the inhibition of axonal regeneration after neuronal injury.

Microglias show morphological changes, including ramified and amaeboid, the latter being regarded as an activated form (Giulian et al., 1986). KS is reportedly expressed in ramified resident microglias, and is suppressed in experimental autoimmune encephalomyelitis, a T-helper type 1 cell-mediated CNS inflammation model (Jander and Stoll, 1996). After cytokines stimulation, expression of MHC class II, a marker of microglial activation, shows a mirror image profile to that of KS (Jander et al., 2000). Thus, interferon-γ induces MHC class II but not KS, while TNF-α induces KS but not MHC class II. In contrast, we and others have shown KS expression induction in microglias close to the injury center after neuronal injury (Jones and Tuszynski, 2002). Furthermore, KS-deficient mice exhibit more axonal regeneration after a stab wound in the cerebral cortex (Zhang et al., 2006). The present study has also demonstrated that microglias express not only KS but also CS upon stimulation with TGF-β_1. These data indicate that KS expression in microglias is contextual, but that it indicates a hazardous status in some types of CNS injuries.

4. Experimental procedures

4.1. *Controlled cortical knife-cut injury*

C57BL/6J male mice, 8 weeks of age, were maintained in temperature-controlled rooms on a 12 h light/dark cycle. The mice were maintained in the animal facilities of Nagoya University. All experiments were performed in accordance

with protocols approved by the institutional animal committee. C57BL/6J mice were anesthetized and placed in a stereotaxic frame. Cortical injury was induced in the right parietal cortex. For the knife-cut model, a knife cut (2.5 mm depth and 6.0 mm length) 1.0 mm lateral to the bregma was made, and the lesions, the contralateral regions and the corresponding regions from normal mice were isolated at the indicated days after injury.

4.2. *RT-PCR and real-time PCR*

Total RNA was extracted from cells or from brain tissues and was analyzed by RT-PCR and real-time PCR. All the PCR products were taken from the same tissue. GAPDH was used as an internal control to make it sure that the same input amounts were applied for RT-PCR. RT-PCR primers used are summarized in Table 1, under the following PCR conditions: 94 °C for 30 s, 57 °C for 30 s, 72 °C for 1 min, 30 cycles. Real-time PCR was performed using the TaqMan Gene Expression Assays and 7500 Real-time PCR system (Applied Biosystems, Foster, CA). Real-time PCR primers and probes were from Applied Biosystems (GlcNAc6st-1: Assay ID, Mm00490018-gl; β3GlcNACt-7: Assay ID, Mm00507533-ml; C6ST-1: Assay ID, Mm00489736-ml; CS synthase: Assay ID, Mm01319178-ml; aggrecan: Assay ID, Mm00573424-gl; GAPH: Assay ID, Mm03302249-gl).

4.3. *Immunohistochemistry*

Tissues were cut into 5-μm sections with a cryostat and mounted on glass slides. The sections were fixed with cold acetone for 5 min, dried, and then blocked in phosphate-buffered saline (PBS) containing 10% goat serum albumin. Sections were then incubated with monoclonal Cy3-conjugatedovemight at 4 °C or 1 h at room temperature. After rinsing, sections stained with anti-Iba1 antibody were incubated with Cy3-conjugated anti-rabbit IgG (500× dilution; Invitrogen, Carlsbad, CA) for 30 min at room temperature, then rinsed. Monoclonal biotin-conjugated anti-CS CS-56 antibody (Seikagaku, Tokyo, Japan) or monoclonal biotin-conjugated anti-KS 5D4 antibody (Seikagaku) at 100× dilution was then incubated in a blocking solution overnight at 4 °C or 1 h at room temperature. After rinsing, Cy2-conjugated streptavidin (Jackson ImmunoResearch, West Grove, PA) was incubated at 500× dilution for 30 min at room temperature, rinsed, and then mounted with FluorSave (Calbiochem, San Diego, CA) and examined by confocal microscopy (MRC 1024; Bio-Rad Laboratories, Tokyo, Japan).

4.4. *Cell culture*

Primary cultures of cerebral cortical astrocytes were prepared from newborn C57BL/6J mice as previously described (Smith et al., 1990; Allaman et al., 2004). Briefly, forebrains were removed aseptically from the skulls, the meninges were excised carefully under a dissecting microscope, and the cortices were isolated. The small tissues obtained by mincing the cortices were cultured in flasks in DMEM containing 10% FCS, then incubated at 37 °C in a humidified atmosphere containing 5% CO_2. The culture medium was renewed every 3–5 days. Experiments were performed on confluent 30-day-old cultures. Over 95% of cells obtained were GFAP-positive. Astrocyte cells were used in 5×10^5 cells in a 3.5-cm dish.

Microglia-enriched cultures were obtained using the method of Giulian et al. (1986). Briefly, small pieces of tissues were obtained by mincing the cortices as described for the astrocyte primary culture and then were cultured in flasks in Mi-medium (DMEM, 10% FCS, 0.2% glucose and insulin 5 μg/ml). The mixed glial culture grown for 21 days was subjected to shaking at 200 rpm on a gyratory shaker for 30 min. The

Table 1 – Nucleotide sequence of RT-PCR primers for target genes

Gene name	Forward primer (5′–3′)	Reverse primer(5′–3′)
GlcNAc6ST-1	AAGCCTACAGGTGGTGCGAA	CAGGACTGTTAACCCGCTCA
GlcNAc6ST-2	TTCTCAGCCTGCAGGCCCTCT	GTTCTTGTTGAGATCTGACCT
GlcNAc6ST-3	AGACAGCCAAGGCGCTGGCA	AACTGTCCATGCCTCTTGGC
GlcNAc6ST-4	TGGTGGTCATCAAAGACGTG	GTCATATTGAATGCGAAGGC
β3GlcNAcT-7	CTATGCTGACATCCTACAGT	ACTTGTGTACCACAAGCATG
β4GalT-4	AGAACTGGGACTGCTTCGTA	TGGCATATAAAGGGTTGTGC
KSGal6ST-1	ATGATTGTGATCTCTACTTT	TTCTGTCTTCTTCATTGGAT
C4ST-1	ACTCATCTACTGCTATGTGC	CCTCCAGTGTCTCATACTTG
C6ST-1	ACCACTTGACTCAGTTC	TGCGTGTTCTTCTGGATC
GalNAcT-1	AGGCGGCTTGCAGAAGTATG	CCTCTGTGGCTTTATCCAGG
GalNAc4,6ST	GAAGATTACCTGGACCTCTT	GTGCATGGTATACTTGACAT
2OST	CATGTCCACTTCCTCAACTT	CGTAGTGGTAGAACTCGTAC
GlcAT-1	AGGTACAGGATGGCCGCGTT	TGTAGCTGCTCCTCCTGCTT
CS synthase-1	TGACATGCAGGTCCTGCCTG	AGAGGTCCACATCCTCCAGC
XylT-1	GCATCCACACCCTCAGCGAT	GCTGCAATGACGTTGACAGG
GalT-1	CGACCGTAATGCCTACAGGT	CCGGTCAAACCTCTGAGGAT
GalT-2	CTTTGCCATCGCCATGGACA	AATGCCGTCCCACTTCATGC
Aggrecan	CAGGGTCACTGTTACCGGCA	GTGCAGGTGATTCGAGGCTC
EGF	TCCTAGAGAAACACCAAGAC	AGCAGTGATTAGCCGTGGAA
bFGF	ACACGTCAAACTACAACTCC	CATTGGAAGAAACAGTATGG
TGF-β_1	CACCATCCATGACATGAACC	GCACAATCATGTTGGACAA
GAPDH	GGTGGAGGTCGGAGTCAACG	CAAAGTTGTCATGGATGACC

detached cells (mainly microglia) were reseeded in fresh culture flasks, and after 2 h any contaminating oligodendrocyte progenitors were detached with Tris-buffered saline containing 1 mM EDTA. This procedure routinely provides a firmly attached homogeneous population of microglia. Microglia were cultured in DMEM containing 10% FBS. More than 95% of cells obtained were found to be Iba1-positive. Microglial cells were used in 1×10^5 cells in a 3.5-cm dish.

In all experiments, microglias and astrocytes were grown for an additional 24 h after cytokines were added: IL-1β 10 ng/ml (Sigma), TNF-α 20 ng/ml (PeproTech House, London, UK), TGF-β_1 35 ng/ml (R&D, Minneapolis, MN), EGF 20 ng/ml (Biomedical Technologies Inc., Stoughton, MA) or bFGF 20 ng/ml (PeproTech House, London, UK) or conditioned medium.

4.5. *Western blot analysis*

Samples of the supernatant fraction and cells were collected after centrifuging at 10,000 *g* for 15 min and were separated by electrophoresis on 5% SDS–PAGE. Proteins were then blotted onto nitrocellulose membranes. Blots were blocked with 5% fat-free dry milk in PBS for 60 min and incubated overnight at 4 °C with the primary antibody [anti-KS 5D4 (1000×dilution; Seikagaku), anti-CS CS56 (1000×dilution; Seikagaku) or anti-aggrecan (1000×dilution)] in PBS containing 0.3% Triton X-100. They were washed and then were incubated with a second antibody [horseradish peroxidase-conjugated goat anti-mouse IgG (5000× dilution), anti-mouse IgM (5000×dilution) or anti-rabbit IgG (5000×dilution; Jackson ImmunoResearch)] in PBS containing 0.3% Triton X-100 at room temperature for 60 min. Anti-bFGF antibody (1000×dilution; Biomedical Technologies, Stoughton, MA) and anti-β-actin antibody (100,000×dilution; Sigma) were also used as indicated. Bound antibodies were visualized with an ECL Western blotting detection kit (GE Healthcare, Buckinghamshire, UK).

4.6. *Enzymatic treatment*

Before immunohistochemistry and Western blotting by the use of 5D4 (anti-KS) antibody were performed, tissue specimens or cell media were treated with chondroitinase ABC (1 mU/μg protein, 0.1 M Tris–acetate, pH 7.3; Seikagaku) overnight at 37 °C.

4.7. *Quantification of TGF-β_1 and TGF-β_1-neutralizing antibody*

The amounts of TGF-β_1 were estimated by ELISA (R&D, Minneapolis, MN). TGF-β_1-neutralizing monoclonal antibody (HB 9849, ATCC, Manassas, VA) was obtained from the American Type Culture Collection (Manassas, VA); normal mouse IgG was from Invitrogen. Anti-TGF-β_1 or normal mouse IgG at 5 μg/ml was added to the microglia medium stimulated by bFGF-ACM for 24 h. After 24 h, KSPG and CSPG expression in microglias was examined by Western blotting.

4.8. *Statistical analysis*

Statistical analysis was performed using the Student's t-test. $P<0.05$ was considered statistically significant.

Acknowledgments

We thank Hideto Watanabe, Nobuo Sugiura and Kenji Uchimura for their helpful comments on this manuscript, and Takashi Muramatsu for his continuous support of this study. This work was supported by the 21st COE program and the Global COE program, MEXT, Japan; Grants-in-Aid, MEXT (18390099 and 20390092 to K.K.) and by the Uehara Foundation.

REFERENCES

Allaman, I., Pellerin, L., Magistretti, P.J., 2004. Glucocorticoids modulate neurotransmitter-induced glycogen metabolism in cultured cortical astrocytes. J. Neurochem. 88, 900–908.

Araujo, D.M., Cotman, C.W., 1992. Basic FGF in astroglial, microglial, and neuronal cultures: characterization of binding sites and modulation of release by lymphokines and trophic factors. J. Neurosci. 12, 1668–1678.

Asher, R.A., Morgenstern, D.A., Fidler, P.S., Adcock, K.H., Oohira, A., Braistead, J.E., Levine, J.M., Margolis, R.U., Rogers, J.H., Fawcett, J.W., 2000. Neurocan is upregulated in injured brain and in cytokine-treated astrocytes. J. Neurosci. 20, 2427–2438.

Bradbury, E.J., Moon, L.D., Popat, R.J., King, V.R., Bennett, G.S., Patel, P.N., Fawcett, J.W., McMahon, S.B., 2002. Chondroitinase ABC promotes functional recovery after spinal cord injury. Nature 416, 636–640.

Brambilla, R., Cottini, L., Fumagalli, M., Ceruti, S., Abbracchio, M.P., 2003. Blockade of A2A adenosine receptors prevents basic fibroblast growth factor-induced reactive astrogliosis in rat striatal primary astrocytes. Glia 243, 190–194.

De Winter, F., Holtmaat, A.J., Verhaagen, J., 2002. Neuropilin and class 3 semaphorins in nervous system regeneration. Adv. Exp. Med. Biol. 515, 115–139.

Dobbertin, A., Rhodes, K.E., Garwood, J., Properzi, F., Heck, N., Rogers, J.H., Fawcett, J.W., Faissner, A., 2003. Regulation of RPTPbeta/phosphacan expression and glycosaminoglycan epitopes in injured brain and cytokine-treated glia. Mol. Cell. Neurosci. 24, 951–971.

Emerling, D.E., Lander, A.D., 1996. Inhibitors and promoters of thalamic neuron adhesion and outgrowth in embryonic neocortex: functional association with chondroitin sulfate. Neuron 17, 1089–1100.

Endoh, M., Pulsinelli, W.A., Wagner, J.A., 1994. Transient global ischemia induces dynamic changes in the expression of bFGF and the FGF receptor. Brain Res. Mol. Brain Res. 22, 76–88.

Faber-Elman, A., Solomon, A., Abraham, J.A., Marikovsky, M., Schwartz, M., 1996. Involvement of wound-associated factors in rat brain astrocyte migratory response to axonal injury: in vitro simulation. J. Clin. Invest. 97, 162–171.

Filbin, M.T., 2003. Myelin-associated inhibitors of axonal regeneration in the adult mammalian CNS. Nat. Rev. Neurosci. 4, 703–713.

Giulian, D., Baker, T.J., Shih, L.C., Lachman, L.B., 1986. Interleukin 1 of the central nervous system is produced by ameboid microglia. J. Exp. Med. 164, 594–604.

Grimpe, B., Silver, J., 2004. A novel DNA enzyme reduces glycosaminoglycan chains in the glial scar and allows microtransplanted dorsal root ganglia axons to regenerate beyond lesions in the spinal cord. J. Neurosci. 24, 1393–1397.

Gross, C.E., Bednar, M.M., Howard, D.B., Sporn, M.B., 1993. Transforming growth factor-beta 1 reduces infarct size after experimental cerebral ischemia in a rabbit model. Stroke 24, 558–562.

Habuchi, H., Habuchi, O., Uchimura, K., Kimata, K., Muramatsu, T., 2006. Determination of substrate specificity of

sulfotransferases and glycosyltransferases (proteoglycans). Methods Enzymol. 416, 225–243.
Hata, K., Fujitani, M., Yasuda, Y., Doya, H., Saito, T., Yamagishi, S., Mueller, B.K., Yamashita, T., 2006. RGMa inhibition promotes axonal growth and recovery after spinal cord injury. J. Cell Biol. 173, 47–58.
Henrich-Noack, P., Prehn, J.H., Krieglstein, J., 1996. TGF-beta 1 protects hippocampal neurons against degeneration caused by transient global ischemia. Dose–response relationship and potential neuroprotective mechanisms. Stroke 27, 1609–1614 discussion 1615.
Jander, S., Stoll, G., 1996. Downregulation of microglial keratan sulfate proteoglycans coincident with lymphomonocytic infiltration of the rat central nervous system. Am. J. Pathol. 148, 71–78.
Jander, S., Schroeter, M., Fischer, J., Stoll, G., 2000. Differential regulation of microglial keratan sulfate immunoreactivity by proinflammatory cytokines and colony-stimulating factors. Glia. 30, 401–410.
Johnson-Green, P.C., Dow, K.E., Riopelle, R.J., 1991. Characterization of glycosaminoglycans produced by primary astrocytes in vitro. Glia 4, 314–321.
Jones, L.L., Tuszynski, M.H., 2002. Spinal cord injury elicits expression of keratan sulfate proteoglycans by macrophages, reactive microglia, and oligodendrocyte progenitors. J. Neurosci. 22, 4611–4624.
Kaneko, S., Iwanami, A., Nakamura, M., Kishino, A., Kikuchi, K., Shibata, S., Okano, H.J., Ikegami, T., Moriya, A., Konishi, O., Nakayama, C., Kumagai, K., Kimura, T., Sato, Y., Goshima, Y., Taniguchi, M., Ito, M., He, Z., Toyama, Y., Okano, H., 2006. A selective Sema3A inhibitor enhances regenerative responses and functional recovery of the injured spinal cord. Nat. Med. 12, 1380–1389.
King, V.R., Phillips, J.B., Brown, R.A., Priestley, J.V., 2004. The effects of treatment with antibodies to transforming growth factor beta1 and beta2 following spinal cord damage in the adult rat. Neuroscience 126, 173–183.
Kitayama, K., Hayashida, Y., Nishida, K., Akama, T.O., 2007. Enzymes responsible for synthesis of corneal keratan sulfate glycosaminoglycans. J. Biol. Chem. 282, 30085–30096.
Laabs, T.L., Wang, H., Katagiri, Y., McCann, T., Fawcett, J.W., Geller, H.M., 2007. Inhibiting glycosaminoglycan chain polymerization decreases the inhibitory activity of astrocyte-derived chondroitin sulfate proteoglycans. J. Neurosci. 27, 14494–14501.
Logan, A., Frautschy, S.A., Gonzalez, A.M., Sporn, M.B., Baird, A., 1992. Enhanced expression of transforming growth factor beta 1 in the rat brain after a localized cerebral injury. Brain Res. 587, 216–225.
Logan, A., Baird, A., Berry, M., 1999. Decorin attenuates gliotic scar formation in the rat cerebral hemisphere. Exp. Neurol. 159, 504–510.
McNeill, H., Williams, C., Guan, J., Dragunow, M., Lawlor, P., Sirimanne, E., Nikolics, K., Gluckman, P., 1994. Neuronal rescue with transforming growth factor-beta 1 after hypoxic–ischaemic brain injury. NeuroReport 5, 901–904.
Meiners, S., Marone, M., Rittenhouse, J.L., Geller, H.M., 1993. Regulation of astrocytic tenascin by basic fibroblast growth factor. Dev. Biol. 60, 480–493.
Miller, B., Sheppard, A.M., Pearlman, A.L., 1997. Developmental expression of keratan sulfate-like immunoreactivity distinguishes thalamic nuclei and cortical domains. J. Comp. Neurol. 380, 533–552.
Min, K.J., Yang, M.S., Kim, S.U., Jou, I., Joe, E.H., 2006. Astrocytes induce hemeoxygenase-1 expression in microglia: a feasible mechanism for preventing excessive brain inflammation. J. Neurosci. 26, 1880–1887.
Moon, L.D., Fawcett, J.W., 2001. Reduction in CNS scar formation without concomitant increase in axon regeneration following treatment of adult rat brain with a combination of antibodies to TGFbeta1 and beta2. Eur. J. Neurosci. 14, 1667–1677.
Moon, L.D., Asher, R.A., Rhodes, K.E., Fawcett, J.W., 2001. Regeneration of CNS axons back to their target following treatment of adult rat brain with chondroitinase ABC. Nat. Neurosci. 4, 465–466.
Neumann, S., Woolf, C.J., 1999. Regeneration of dorsal column fibers into and beyond the lesion site following adult spinal cord injury. Neuron 23, 83–91.
Oohira, A., Matsui, F., Tokita, Y., Yamauchi, S., Aono, S., 2000. Molecular interactions of neural chondroitin sulfate proteoglycans in the brain development. Arch. Biochem. Biophys. 374, 24–34.
Perosa, S.R., Porcionatto, M.A., Cukiert, A., Martins, J.R., Passeroti, C.C., Amado, D., Matas, S.L., Nader, H.B., Cavalheiro, E.A., Leite, J.P., Naffah-Mazzacoratti, M.G., 2002. Glycosaminoglycan levels and proteoglycan expression are altered in the hippocampus of patients with mesial temporal lobe epilepsy. Brain Res. Bull. 58, 509–516.
Properzi, F., Carulli, D., Asher, R.A., Muir, E., Camargo, L.M., van Kuppevelt, T.H., ten Dam, G.B., Furukawa, Y., Mikami, T., Sugahara, K., Toida, T., Geller, H.M., Fawcett, J.W., 2005. Chondroitin 6-sulphate synthesis is up-regulated in injured CNS, induced by injury-related cytokines and enhanced in axon-growth inhibitory glia. Eur. J. Neurosci. 21, 378–390.
Ridet, J.L., Malhotra, S.K., Privat, A., Gage, F.H., 1997. Reactive astrocytes: cellular and molecular cues to biological function. Trends Neurosci. 20, 570–577.
Riboni, L., Viani, P., Bassi, R., Giussani, P., Tettamanti, G., 2001. Basic fibroblast growth factor-induced proliferation of primary astrocytes. Evidence for the involvement of sphingomyelin biosynthesis. J. Biol. Chem. 276, 12797–12804.
Ruoslahti, E., 1996. Brain extracellular matrix. Glycobiology 6, 489–492.
Sakai, K., Kimata, K., Sato, T., Gotoh, M., Narimatsu, H., Shinomiya, K., Watanabe, H., 2007. Chondroitin sulfate N-acetylgalactosaminyltransferase-1 plays a critical role in chondroitin sulfate synthesis in cartilage. J. Biol. Chem. 282, 4152–4161.
Schilling, T., Nitsch, R., Heinemann, U., Haas, D., Eder, C., 2001. Astrocyte-released cytokines induce ramification and outward K+ channel expression in microglia via distinct signalling pathways. Eur. J. Neurosci. 14, 463–473.
Scott, J.E., Cummings, C., Greiling, H., Stuhlsatz, H.W., Gregory, J. D., Damle, S.P., 1990. Examination of corneal proteoglycans and glycosaminoglycans by rotary shadowing and electron microscopy. Int. J. Biol. Macromol. 12, 180–184.
Silbert, J.E., Sugumaran, G., 2002. Biosynthesis of chondroitin/dermatan sulfate. IUBMB Life 54, 177–186.
Silver, J., Miller, J.H., 2004. Regeneration beyond the glial scar. Nat. Rev. Neurosci. 5, 146–156.
Smith, G.M., Strunz, C., 2005. Growth factor and cytokine regulation of chondroitin sulfate proteoglycans by astrocytes. Glia 52, 209–218.
Smith, G.M., Rutishauser, U., Silver, J., Miller, R.H., 1990. Maturation of astrocytes in vitro alters the extent and molecular basis of neurite outgrowth. Dev. Biol. 138, 377–390.
Snow, D.M., Steindler, D.A., Silver, J., 1990. Molecular and cellular characterization of the glial roof plate of the spinal cord and optic tectum: a possible role for a proteoglycan in the development of an axon barrier. Dev. Biol. 138, 359–376.
Vincent, V.A., Tilders, F.J., Van Dam, A.M., 1997. Inhibition of endotoxin-induced nitric oxide synthase production in microglial cells by the presence of astroglial cells: a role for transforming growth factor beta. Glia 19, 190–198.
Vincent, V.A., Lowik, C.W., Verheijen, J.H., de Bart, A.C., Tilders, F.J., Van Dam, A.M., 1998. Role of astrocyte-derived tissue-type plasminogen activator in the regulation of

endotoxin-stimulated nitric oxide production by microglial cells. Glia 22, 130–137.
Wang, Y., Moges, H., Bharucha, Y., Symes, A., 2007. Smad3 null mice display more rapid wound closure and reduced scar formation after a stab wound to the cerebral cortex. Exp. Neurol. 203, 168–184.
Widenfalk, J., Lundstromer, K., Jubran, M., Brene, S., Olson, L., 2001. Neurotrophic factors and receptors in the immature and adult spinal cord after mechanical injury or kainic acid. J. Neurosci. 21, 3457–3475.
Wiessner, C., Gehrmann, J., Lindholm, D., Töpper, R., Kreutzberg, G.W., Hossmann, K.A., 1993. Expression of transforming growth factor-beta 1 and interleukin-1 beta mRNA in rat brain following transient forebrain ischemia. Acta Neuropathol. 86, 439–446.
Wyss-Coray, T., Feng, L., Masliah, E., Ruppe, M.D., Lee, H.S., Toggas, S.M., Rockenstein, E.M., Mucke, L., 1995. Increased central nervous system production of extracellular matrix components and development of hydrocephalus in transgenic mice overexpressing transforming growth factor-beta 1. Am. J. Pathol. 147, 53–67.
Zhang, H., Muramatsu, T., Murase, A., Yuasa, S., Uchimura, K., Kadomatsu, K., 2006. N-Acetylglucosamine 6-O-sulfotransferase-1 is required for brain keratan sulfate biosynthesis and glial scar formation after brain injury. Glycobiology 16, 702–710.

Journal of Neuroscience Research 87:2908–2915 (2009)

Disruption of the Midkine Gene (Mdk) Delays Degeneration and Regeneration in Injured Peripheral Nerve

Harutoshi Sakakima,[1]* Yoshihiro Yoshida,[1] Yoshiki Yamazaki,[1] Fumiyo Matsuda,[1] Masako Ikutomo,[1] Kosei Ijiri,[2] Hisako Muramatsu,[3] Takashi Muramatsu,[3] and Kenji Kadomatsu[3]

[1]School of Health Sciences, Faculty of Medicine, Kagoshima University, Kagoshima, Japan
[2]Department of Orthopaedic Surgery, Kagoshima University, Kagoshima, Japan
[3]Department of Biochemistry, School of Medicine, Nagoya University, Nagoya, Japan

Midkine (MK) is a growth factor implicated in the development and repair of various tissues, especially neural tissues. MK acts as a reparative neurotrophic factor in damaged peripheral nerves. A postulated role of MK in the degeneration and regeneration of sciatic nerves was explored by comparing wild-type ($Mdk^{+/+}$) mice with MK-deficient ($Mdk^{-/-}$) mice after freezing injury. In the $Mdk^{-/-}$ mice, a regenerative delay was observed, preceded by a decelerated Wallerian degeneration (WD). The relative wet weight of the soleus muscle slowly declined, and recovery was delayed compared with that in the $Mdk^{+/+}$ mice. In the regenerating nerve, unmyelinated axons were unevenly distributed, and some axons contained myelin-like, concentrically lamellated bodies. In the endplates of soleus muscles, nerve terminals containing synaptic vesicles disappeared in both mice. In $Mdk^{-/-}$ mice, the appearance of nerve terminals was delayed in synaptic vesicles of terminal buttons after injury. The recovery of evoked electromyogram was delayed in $Mdk^{-/-}$ mice compared with $Mdk^{+/+}$ mice. Our results suggested a delay in axonal degeneration and regeneration in $Mdk^{-/-}$ mice compared with $Mdk^{+/+}$ mice, and the delayed regeneration was associated with a delayed recovery of motor function. These findings show that a lack of MK following peripheral nerve injury is a critical factor in degeneration and regeneration, and manipulation of the supply of MK may offer interesting therapeutic options for the treatment of peripheral nerve damage.

Key words: midkine; knockout mice; sciatic nerve; nerve regeneration; Wallerian degeneration

Damage to a peripheral nerve initiates a broad range of events in the proximal and distal stump of the nerve. Growth factors play key roles in the control of development by regulating the growth, differentiation, and survival of various types of cells. Various neurotrophic factors are important for the recovery of neuronal functions following crush and transection nerve injury, such as nerve growth factor (NGF), brain-derived neurotrophic factor (BDNF), and ciliary neurotrophic factor (CNTF; Yamamoto et al., 1993). These factors are released from Schwann cells, and a gradient develops around regenerating axons (Ide, 1996). Midkine (MK) and transforming growth factor (TGF)-β2 are anterogradely transported in the axonal flow after peripheral nerve injury (Jiang et al., 2000; Sakakima et al., 2004b).

MK is a member of a family of developmentally regulated neurotrophic and heparin binding growth factors (Kadomatsu et al., 1988). MK is expressed during the midgestation period in a retinoic-acid dependent manner during embryogenesis in the mouse (Kadomatsu et al., 1988, 1990; Huang et al., 1990). MK enhances the growth, survival, and migration of various cells (Michikawa et al., 1992; Muramatsu et al., 1993; Muramatsu, 2002; Maruyama et al., 2004) and expressed in senile plaques of the brain in patients with Alzheimer's disease (Yasuhara et al., 1993), in the areas surrounding cerebral infarct (Yoshida et al., 1995) in injured spinal cords of rats (Sakakima et al., 2004a,b), and in various human neoplasms (Tsutsui et al., 1993). Studies of the physiological role of MK in the central nervous system suggest neurotrophic effects (Yoshida et al., 2001; Wada et al., 2002). In addition, MK expression is found in bone repair (Ohta et al., 1999) and skeletal muscle regeneration (Sakakima et al., 2006). MK is a multifunctional cytokine with neurotrophic activity.

The essential role of MK in the growth, survival, and migration of various cells has been shown using mice deficient in the MK gene ($Mdk^{-/-}$ mice; Sato

Contract grant sponsor: Japanese Ministry of Culture, Education, and Science; Contract grant number: 19700434 (to H.S.).

*Correspondence to: Harutoshi Sakakima, PhD, School of Health Sciences, Faculty of Medicine, Kagoshima University, 8-35-1 Sakuragaoka, Kagoshima, 890-8544 Japan. E-mail: sakaki@health.nop.kagoshima-u.ac.jp

Received 26 January 2009; Revised 12 March 2009; Accepted 14 April 2009

Published online 12 May 2009 in Wiley InterScience (www.interscience.wiley.com). DOI: 10.1002/jnr.22127

et al., 2001; Maruyama et al., 2004). $Mdk^{-/-}$ mice exhibit retarded postnatal development in the hippocampus (Nakamura et al., 1998). Morphological changes and macrophage infiltration of tubulointerstitial damage of diabetic nephropathy were strikingly less extensive in $Mdk^{-/-}$ mice than in $Mdk^{+/+}$ mice (Kosugi et al., 2007). We previously demonstrated that MK was produced by axotomized motor neurons and might act as a reparative neurotrophic factor in damaged peripheral nerve (Sakakima et al., 2004b). However, little is known about the role of MK in peripheral nerve injury. Therefore, we investigated the difference between midkine knockout and wild-type mice in the degeneration and regeneration of peripheral nerve by conducting histological and electrophysiological assessments.

MATERIALS AND METHODS

MK-Deficient Mice

A basic targeting vector with MC1neo (polyoma virus thymidine kinase gene promoter and neomycin resistance gene), PGK (phosphoglucokinase gene promoter), and DTA (diphtheria toxin fragment A gene) was constructed as described previously (Igakura et al., 1998). The generation of $Mdk^{-/-}$ 129/SV mice has been described previously (Nakamura et al., 1998). After the back-crossing of $Mdk^{+/-}$ mice to C57/BL mice for seven generations, the $Mdk^{+/-}$ mice were mated with each other to generate $Mdk^{+/+}$ (wild-type mice) and $Mdk^{-/-}$ mice, which were used in the present study. All experiments were performed with $Mdk^{+/+}$ and $Mdk^{-/-}$ littermates. Mice used were 8–10-week-old males and were fed normal rodent chow.

Polymerase Chain Reaction

PCR was performed as described previously (Igakura et al., 1998). For the screening of F1 mice with homologously recombined DNA, Neo primers were used: forward, 5′-GTG TGGTTTTGCAAGAGGAAG-3′; reverse, 5′-CCTGCGTGC AATCCATCTTG-3′. The wild-type DNA gave no band, whereas the recombined DNA gave a 352-bp band. For the screening of F2 mice, MK primers were used: forward, 5′-TAACCCAGGTTTTACCCCTA-3′; reverse, 5′-CTCCAAA TTCCTTCCTTCTTCCAG-3′. The wild-type DNA gave a 372-bp band, and the recombined DNA gave a 1,297-bp band.

Induction of Sciatic Nerve Injury and Preparation of Specimens

Male $Mdk^{+/+}$ and $Mdk^{-/-}$ mice weighing 20–30 g were anesthetized with an intraperitoneal injection of sodium pentobarbital (30 mg/kg). The skin covering the right buttock was cut. The right sciatic nerve was exposed and separated from the surrounding tissues. The nerve was frozen and thawed 10 times at 10-sec intervals through contact with a stainless steel spatula 1 mm in diameter cooled with liquid nitrogen. Care was taken not to injure the other tissues. Freezing was chosen as the method of denervation because it uniformly and definitively damages nerve fibers with reinnervation more than other procedures such as nerve crush or transection (Sakakima et al., 2000). The nerve became white when frozen, and the proximal margin of the frozen portion was loosely tied with a white thread for marking. Contralateral hindlimbs were untreated and served as controls. Animals were housed under temperature-controlled conditions at 22°C ± 1°C on a 12-hr reverse light and dark cycle with food and water available ad libitum. The degree of paralysis of the hindlimbs in the treated mice was checked daily. The $Mdk^{+/+}$ and $Mdk^{-/-}$ mice were sacrificed 1 (n = 5), 2 (n = 5), 3 (n = 6), 4 (n = 4), and 5 (n = 3) weeks after sciatic nerve freezing. Additionally, three intact $Mdk^{+/+}$ and $Mdk^{-/-}$ mice were sacrificed as controls. Efforts were made to reduce the number of animals used.

Mice were perfused transcardially with physiological saline under deep ether anesthesia. Subsequently, soleus muscles from both legs and accompanying sciatic nerves of the frozen sides were removed. The distance between the white thread for marking and the nerve's entrance into the soleus muscle was measured and was 10.8 ± 0.9 mm (mean ± SD). The bilateral soleus muscles were removed, and their wet weight was measured to monitor reinnervation after the injury. The sciatic nerve was divided into proximal and distal portions relative to the lesion. The portion distal to the lesion and the soleus muscles were used for the electron microscopic analysis. Material for histology and morphometry was taken about 5.0 mm distal to the lesion. We observed the change to motor endplates of soleus muscle and the distal sciatic nerve in order to examine the regeneration after freezing. The experimental protocol was approved by the ethical board of the Institute of Laboratory Animal Sciences of Kagoshima University.

Electron Microscopy

The soleus muscles and distal portions of the sciatic nerve of $Mdk^{+/+}$ and $Mdk^{-/-}$ mice were immersed in 3% glutaraldehyde in 0.1 M phosphate buffer (pH 7.4) at 4°C overnight. The specimens were postfixed in 1% OsO_4 in 0.1 M phosphate buffer (pH 7.4) overnight at 4°C, rinsed in 10% saccharose three times (10 min each), and stained en bloc in 3% aqueous uranyl acetated for 1 hr at room temperature. Samples were then dehydrated in an ascending series of ethanol concentrations, replaced by propulene oxide, and embedded in epoxy resin. Three blocks were selected at random from each soleus muscle. Semithin sections of soleus muscle and sciatic nerve were cut, stained with 0.5% toluidine blue in 0.5% borate, and observed under a conventional light microscope to examine the reinnervation. Ultrathin sections were cut, stained with uranyl acetate and lead citrate, and observed with an electron microscope (Hitachi H-7100). All endplates observed were photographed and analyzed.

Electrophysiological Analysis

An additional four $Mdk^{+/+}$ and four $Mdk^{-/-}$ mice were used to examine functional recovery. The recovery of nerve function was recorded using an evoked electromyogram (EMG) system (Neuropack μ QP-909B; Nihon Koden, Japan). The right sciatic nerve was exposed and frozen with sodium pentobarlbital (30 mg/kg) by the same procedure.

Electrical stimulation of the sciatic nerve was used to analyze evoked EMG of denervated nerve-muscle units. The $Mdk^{+/+}$ and $Mdk^{-/-}$ mice were stimulated 1 hr and 1, 2, 3, 4, and 5 weeks after sciatic nerve freezing under anesthesia. The sciatic nerve was stimulated 3–5 mm from the sciatic nerves lesion using a bipolar needle electrode. The electrode was inserted in a depth of 3 mm into the skin. The electromyographic signals of the soleus or gastrocnemius muscles during electrical stimulation were recorded using a bipolar needle electrode. The recording electrode was inserted 2–3 mm into the skin. The sciatic nerve was stimulated at a rate of 1 Hz and an intensity of 0.4 mA. Amplitude was measured to examine the tension of isometric twitches of calf muscles during the electrical stimulation. In addition, we checked the ankle joint movement during the stimulation.

Data Analysis

Statistical analyses were performed in StatView version 5.0. Values for means of muscle wet weight and amplitude of EMG signals were compared by one-way ANOVA. If significance was achieved ($P < 0.05$), a post hoc Fisher's protected least significant differences (PLSD) test was performed to determine where significant differences existed. Unpaired Student's *t*-tests were also used to determine differences between $Mdk^{+/+}$ and $Mdk^{-/-}$ mice. Significance was set at $P < 0.05$.

RESULTS

No clinical signs of pain or discomfort were observed over the regeneration period. After freezing of nerve, $Mdk^{+/+}$ and $Mdk^{-/-}$ mice remained ambulatory, although they dragged their foot on the frozen side. Loss of active movement of the ankle and toe joints was observed in both mice. In $Mdk^{+/+}$ mice, almost no voluntary extension of digits was noticed until 2 weeks. After 3 weeks, the active spreading of digits and flexion of the ankle joint was clearly observed. $Mdk^{-/-}$ mice started to spread their digits after 4 weeks. After 5 weeks, the active spreading of digits was clearly observed, although flexion of the ankle joint was still weaker than on the contralateral side and on the ipsilateral side of $Mdk^{+/+}$ mice.

Wet Weight of Soleus Muscles

Soleus muscle wet weights of control $Mdk^{+/+}$ and $Mdk^{-/-}$ mice were 6.4 ± 1.3 mg and 7.5 ± 0.8 mg, respectively; there was no significant difference between $Mdk^{+/+}$ and $Mdk^{-/-}$ mice. To minimize individual and age-related differences in treated mice, the wet weights of denervated/reinnervated soleus muscles were expressed as percentages of those of the contralateral soleus muscles. The relative wet weight showed a different pattern in $Mdk^{+/+}$ and $Mdk^{-/-}$ mice (Fig. 1). The relative wet weight in $Mdk^{-/-}$ mice slowly declined, and the recovery was delayed compared with that in $Mdk^{+/+}$ mice. In the $Mdk^{+/+}$ mice, a faster loss of soleus muscle mass was found, with a maximum in 1 week after freezing. This trend was reversed from 2 weeks after injury. In the $Mdk^{-/-}$ mice, the wet weight of the denervated soleus muscle declined, reaching a minimum 3 weeks after injury. This trend was reversed from 4 weeks. The relative muscle wet weight was significantly greater than that of $Mdk^{+/+}$ mice 1 week after injury ($P < 0.05$).

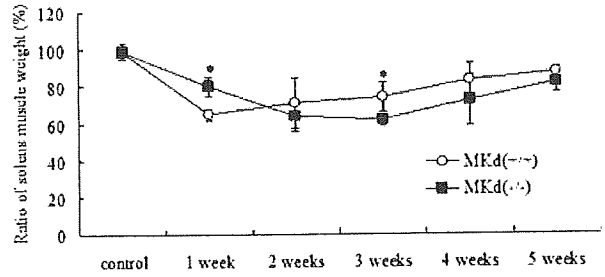

Fig. 1. Weight of the soleus muscle relative to the intact contralateral side. In $Mdk^{+/+}$ mice, a faster loss of muscle mass was noted, with a maximum at 1 week after nerve freezing. In $Mdk^{-/-}$ mice, muscle atrophy was generally delayed. Values are mean ± SD. $*P < 0.05$ between the $Mdk^{+/+}$ and $Mdk^{-/-}$ groups.

Morphogical Analysis of Sciatic Nerve

$Mdk^{-/-}$ mice showed evidence of a delay in Wallerian degeneration (WD), preceded by the slowing of axonal degeneration. At the light microscopic level, uninjured sciatic nerve in $Mdk^{+/+}$ and $Mdk^{-/-}$ mice consists of large and small axons (Fig. 2A,B). Most of the myelin in $Mdk^{+/+}$ mice had clearly degenerated, and the myelin sheaths where axons had previously been located were densely stained 1 week after injury (Fig. 2C). A few thin myelin formations surrounding small light centers were observed 2 weeks after injury (Fig. 2E). After 3, 4, and 5 weeks, the number and area of these regenerated axons increased (Fig. 2G,I). In $Mdk^{-/-}$ mice, most of the myelin was uniformly damaged, and the myelin sheaths where axons had previously been located were densely stained 1 week after injury (Fig. 2D). Two weeks after injury, the most myelin had mostly degenerated and considerable numbers of macrophages, probably containing myelin debris, were observed (Fig. 2F). However, regenerated axons were seldom observed 2 weeks after injury. At 3 weeks, numerous small myelin formations surrounding small, light centers reappeared (Fig. 2H). At 4 weeks, the number and area of these regenerated axons increased (Fig. 2J). The best regeneration was observed in the 5-week groups. Most axonal cross-sectional areas were smaller in both groups than in the control.

At the electron microscopic level, uninjured sciatic nerve in $Mdk^{+/+}$ and $Mdk^{-/-}$ mice consists of rather large axons, with interspersed groups of unmyelinated axons (Fig. 3A,B). Most myelin in $Mdk^{+/+}$ mice had clearly degenerated, and all myelin sheaths showed irregular profiles, myelin ovoids, and debris 1 week after injury. Schwann cells were hypertrophied, containing

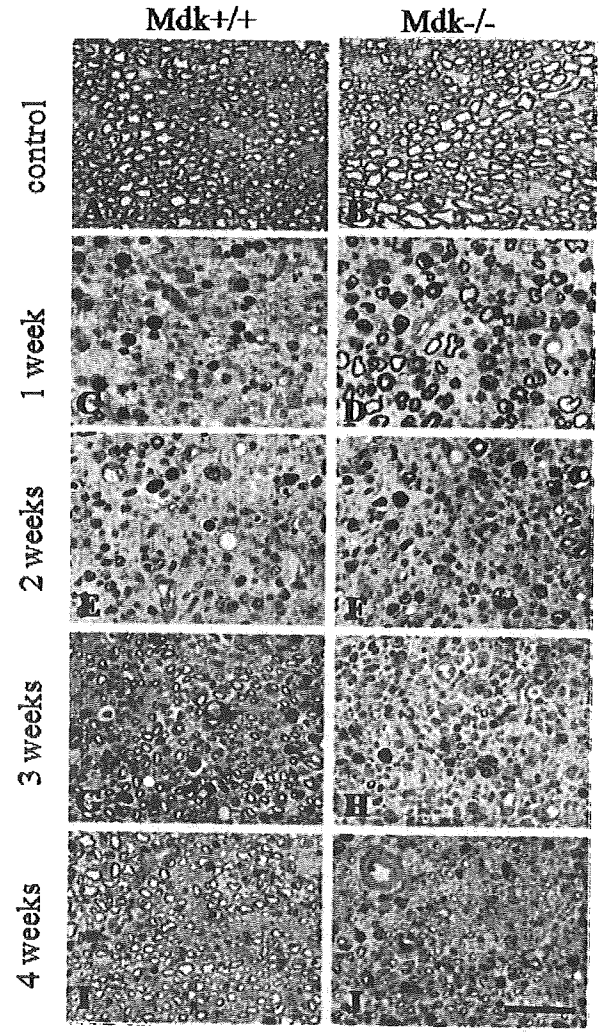

Fig. 2. Representative light micrographs of distal nerve cross-sections. Normal control (**A,B**) and after 1 week (**C,D**), 2 weeks (**E,F**), 3 weeks (**G,H**), and 4 weeks (**I,J**). Intact sciatic nerve in $Mdk^{+/+}$ and $Mdk^{-/-}$ mice consists of large and small axons (A,B). In $Mdk^{+/+}$ mice, most myelin was clearly degenerated, and the myelin sheaths were densely stained (C). A few thin myelin formations surrounding small, light centers were observed (E), and the number and area of regenerated axons increased thereafter (G,I). In $Mdk^{-/-}$ mice, most myelin was uniformly damaged, and the myelin sheaths were densely stained (D). Degeneration was delayed compared with that in $Mdk^{+/+}$ mice. Most myelin had degenerated, and considerable numbers of macrophages, probably containing myelin debris, were observed (F). Numerous small myelin formations surrounding small, light centers reappeared (H), and the number and area of these regenerated axons increased (J). Scale bar = 30 μm.

lipid droplets and myelin whorls 1 week after injury (Fig. 3C,E,F). In $Mdk^{-/-}$ mice, the abnormal persistence of intact neurofilaments, apparently myelinated fiber profiles, and fewer phagocytic Schwann cells were found. These observations suggest that WD was decelerated compared with the case in $Mdk^{+/+}$ mice (Fig. 3D,G). Electron microscopic evaluation indicated some structural alterations in regenerated axons. Five weeks after injury in $Mdk^{+/+}$ mice, myelinated and unmyelinated axons coexisted as normal (Fig. 3H). In $Mdk^{-/-}$ mice, unmyelinated axons were unevenly distributed. Some axons included myelin-like, concentrically lamellated bodies (Fig. 3I).

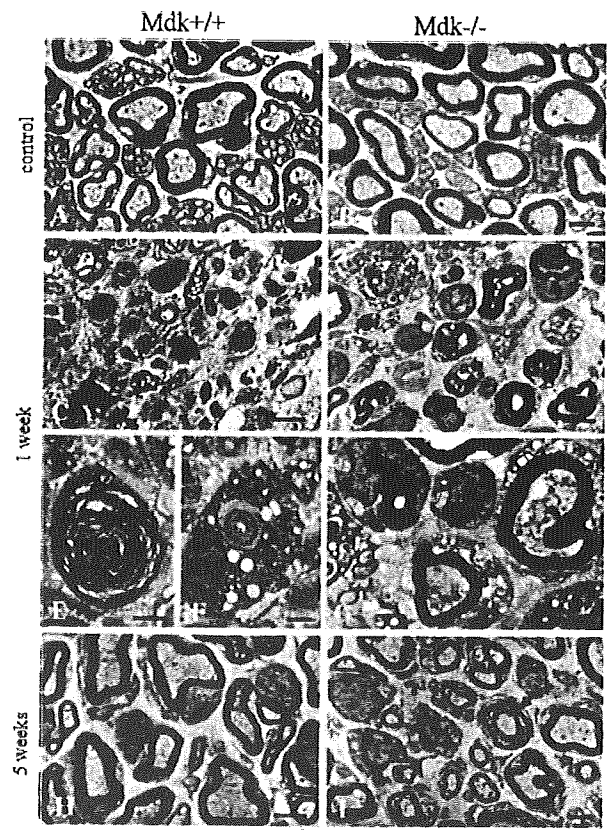

Fig. 3. Representive electron micrographs of distal nerve stumps. Normal control (**A,B**) and after 1 week (**C–G**) and 5 weeks (**H,I**). Intact sciatic nerve in $Mdk^{+/+}$ and $Mdk^{-/-}$ mice consist of rather large axons, with interspersed groups of unmyelinated axons (A,B). In $Mdk^{+/+}$ mice, most myelin had clearly degenerated, and all myelin sheaths showed irregular profiles (C), myelin ovoids (E), and debris. Schwann cells were hypertrophied, containing lipid droplets and myelin whorls (F). Five weeks after injury, myelinated and unmyelinated axons coexisted as normal (H). In $Mdk^{-/-}$ mice, the abnormal persistence of intact neurofilaments, apparently myelinated fibers, and fewer phagocytic Schwann cells were found (D,G). Five weeks after injury, unmyelinated axons were unevenly distributed, and some axons included myelin-like, concentrically lamellated bodies (arrow; I). Scale bars = 5 μm in C,D; 2 μm in A,B,E–I.

Morphogical Analysis of Motor Endplates in Soleus Muscle

Numbers of soleus muscle endplates examined at various time intervals are shown in Table I. In normal

TABLE I. Number of Nerve Terminals Examined in Soleus Muscle of $Mdk^{+/+}$ and $Mdk^{-/-}$ Mice

	Control	1 Week	2 Weeks	3 Weeks	4 Weeks	5 Weeks
$Mdk^{+/+}$ (No. of nerve terminals/ No. of endplates examined)	16/16	15/0	14/3	20/20	14/14	10/10
$Mdk^{-/-}$ (No. of nerve terminals/ No. of endplates examined)	16/16	13/0	13/0	16/3	15/15	12/12

soleus muscles, nerve terminals were observed to lie within a depression of the muscle fiber surface. The presynaptic nerve terminals contained numerous synaptic vesicles and a number of mitochondria. There was no difference in morphology between $Mdk^{+/+}$ and $Mdk^{-/-}$ mice. In the $Mdk^{+/+}$ mice, no presynaptic nerve terminals were found at 1 week after injury (Fig. 4A). Postsynaptic folds were devoid of any overlying nerve terminals. Most postsynaptic folds remained essentially unchanged in structure. At 2 weeks after injury, nerve terminals were not found except in a few regenerated endplates (21%, 3 of 14). However, most endplates did not have nerve terminals containing synaptic vesicles (Fig. 4C). At 3 and 4 weeks, all endplates had vesicle-laden nerve terminals that were still smaller than their normal counterparts (Fig. 4E,G). In $Mdk^{-/-}$ mice, no presynaptic nerve terminals were found at 1 and 2 weeks after injury (Fig. 4B,D). At 3 weeks, nerve terminals were mostly absent, although a few small regenerated endplates had vesicle-laden nerve terminals (19%, 3 of 16). However, most endplates did not have nerve terminals containing synaptic vesicles (Fig. 4F). At 4 weeks, all endplates had vesicle-laden nerve terminals that were still smaller than the normal controls, suggesting a delayed reinnervation compared with $Mdk^{+/+}$ mice (Fig. 4H). At 5 weeks, all endplates in both mice had vesicle-laden nerve terminals that were still small compared with controls.

Electrophysiological Recovery

There was no significant difference in EMG between the $Mdk^{+/+}$ and $Mdk^{-/-}$ mice before freezing. A typical profile of the EMG signals from denervated nerve-muscle units evoked by electrical stimulation of the sciatic nerve is shown in Figure 5A. The amplitude of the signals was smaller in $Mdk^{-/-}$ mice than in $Mdk^{+/+}$ until 4 weeks after injury (Fig. 5B). The EMG signals were significantly decreased in both mice after freezing ($P < 0.05$). No signals were observed in the $Mdk^{+/+}$ or $Mdk^{-/-}$ mice at 1 hr postinjury. The signals gradually increased in both mice during the experimental period. EMG signals were weakly detected in both mice 1 week after injury. At 2 weeks, signals were significantly smaller in $Mdk^{-/-}$ mice than in $Mdk^{+/+}$ mice ($P < 0.05$). In $Mdk^{+/+}$ mice, clearly evoked EMG signals were observed at 4 and 5 weeks. In the $Mdk^{-/-}$ mice, few signals were observed 2 and 3 weeks after injury. At 4 weeks, the weak signals were detected. Clearly evoked EMG signals were detected at 5 weeks.

DISCUSSION

Knockout mice lacking MK gene show no gross abnormalities expect that in the dentate gyrus granule cell layer of the hippocampus of infant $Mdk^{-/-}$ mice (Nakamura et al., 1998). In this study, our morphological observations showed no abnormalities in intact $Mdk^{-/-}$ mice.

The findings of this study indicate that MK-deficient mice exhibit delayed axonal degeneration and regeneration and functional recovery compared with wild-type mice. The mice lacking MK showed a regenerative delay, preceded by a decelerated WD. There have been studies on the essential role of neurotrophic factor in peripheral nerve regeneration using gene-deficient mice. A defect of ciliary neurotrophic factor (CNTF) impaired the ability of mice to recover from crushing of the sciatic nerve (Yao et al., 1999). Mice lacking nitric oxide synthase (nNOS) after sciatic nerve transection showed a delay in the breakdown of myelinated fibers, a delay in regeneration, and a delay in the recovery of sensory and motor functions (Keilhoff et al., 2002). A lack of insulin-like growth factor-I resulted in a decrease in motor and sensory nerve conduction velocities following peripheral nerve injury (Gao et al., 1999). The absence of interleukin 6 (IL-6) did not appear to impair recovery from sciatic nerve injury (Inserra et al., 2000). In contrast, nerve regeneration occurred significantly faster in receptor protein tyrosine phoshatase σ (PTPσ)-deficient mice than in wild-type mice after sciatic nerve crush injury (Mclean et al., 2002). Our results suggest that the lack of the MK gene impaired the ability of mice to recover from sciatic nerve injury and that MK was important for the maturation of regenerating myelinated axons in damaged peripheral nerve.

Mice lacking nNOS after sciatic nerve transection showed a delay in the breakdown of myelinated fibers by a decelerated WD (Keilhoff et al., 2002). After the transection of a peripheral nerve, the segment distal to the lesion undergoes WD, characterized by the proliferation and activation of Schwann cells, the recruitment of macrophages and inflammatory cells, and the degradation and clearance of myelin sheaths and severed axons (Reichert et al., 1994). WD is essential for the regeneration of an injured neuron. In MK-deficient mice, fewer phagocytic Schwann cells were found at 1 week than in wild-type mice. This finding may result from a deficiency in the enhancement of the migration of inflammatory cells because of a lack of MK. Our finding suggested that the lack of an MK gene delayed the beakdown of myelinated fibers in WD.

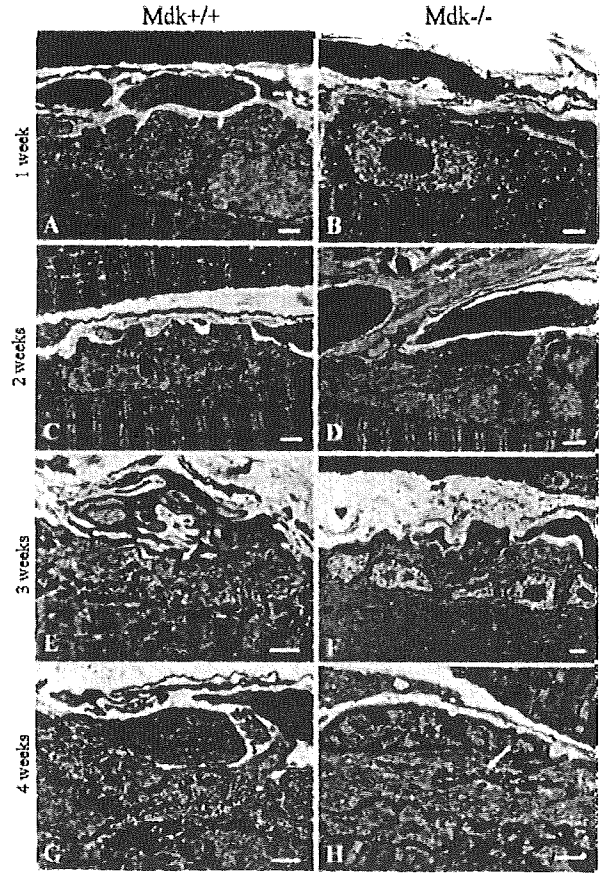

Fig. 4. Electron micrographs of motor endplates in soleus muscle after nerve freezing, after 1 week (**A,B**), 2 weeks (**C,D**), 3 weeks (**E,F**), and 4 weeks (**G,H**). No presynaptic nerve terminals were found until 2 weeks (A–D). In $Mdk^{+/+}$ mice, all endplates had vesicle-laden small nerve terminals at 3 and 4 weeks (short arrow; E,G). In $Mdk^{-/-}$ mice, few presynaptic nerve terminals were found at 3 weeks (F). At 4 weeks, all endplates had vesicle-laden nerve small terminals (long arrow; H). Scale bars = 2 μm.

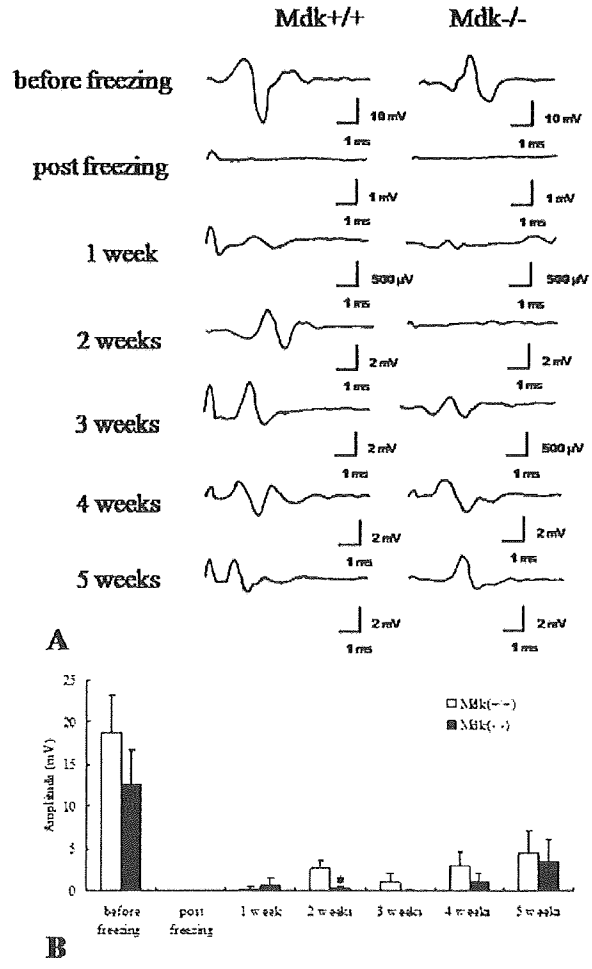

Fig. 5. Typical profile of EMG signals from denervated nerve-muscle units (**A**) and measurement of the amplitude of EMG signals (**B**). The EMG signals gradually strengthened in both mice. The signals were weaker in $Mdk^{-/-}$ mic than in $Mdk^{+/+}$ mice. Values are mean ± SD. $*P < 0.05$ between the $Mdk^{+/+}$ and the $Mdk^{-/-}$ groups.

With MK, pleiotrophin (PTN) forms a family of heparin-binding growth factors. PTN is involved in nerve regeneration and is expressed in Schwann cells, macrophages, and endothelial cells in distal nerve segment but not in axons after peripheral nerve injury (Blondet et al., 2005). We showed that MK was produced in the axotomized motor neurons of the lumbar spinal cord and might act as a reparative neurotrophic factor after sciatic nerve injury (Sakakima et al., 2004b). Ezquerra et al. (2008) demonstrated the different patterns of expression in chronic constriction injury of rat sciatic nerve between MK and PTN. These reports show that expression patterns of MK may be different from the patterns of PTN. Furthermore, MK has various biological activities roles, including in the promotion of inflammatory lekocytes migration (Takada et al., 1997). Histologically defined tubulointerstitial injury was less severe in $Mdk^{-/-}$ mice than in $Mdk^{+/+}$ mice after renal ischemic perfusion injury as a result of less enhancement of the migration of inflammatory cells and the inhibition of inflammation (Sato et al., 2001). On the contrary, administration of PTN to lesioned peripheral nerve delayed macrophage recruitment in the distal crushed nerve (Blondet et al., 2006). These results suggest that the adaptive response to injury is different between MK and PTN. In this study, our results showed that disruption of MK gene delayed degeneration and regeneration after peripheral nerve injury.

After nerve injury from freezing, the reestablishment of original connections is closely associated with the morphological and functional integrity of the skeletal muscle (Sakakima et al., 2000). $Mdk^{+/+}$ mice were

found by light microscopy to have some regenerative axons at 2 weeks after injury. However, no nerve terminals were found in soleus muscle at 2 weeks. Similarly, $Mdk^{-/-}$ mice had regenerative axons at 3 weeks, but no nerve terminals. In addition, the electrophysiological recovery did not accord with the morphological recovery. These results suggest that functional recovery may be delayed compared with a morphological recovery. However, our results showed that the evoked EMG were smaller in $Mdk^{-/-}$ mice than in $Mdk^{+/+}$ mice. Our findings suggest that the MK-deficient mice had a delayed functional recovery after peripheral nerve injury.

Although $Mdk^{-/-}$ mice showed a delay in axonal degeneration and regeneration, they showed regeneration from 4 weeks after injury. At 5 weeks, no significant difference was observed in morphological change and functional recovery between $Mdk^{+/+}$ and $Mdk^{-/-}$ mice. It is likely that many growth factors have overlapping functions so that there are alternative pathways. It is less likely that deletion of a single neurotrophic factor would cause any dramatic disturbance in the regeneration. This study suggested MK to be one of the important neurotrophic factors involved in axonal degeneration and regeneration.

In conclusion, the results presented here suggest that axonal degeneration and regeneration, and functional recovery, are delayed in MK-deficient mice. The local release of MK following damage to a peripheral nerve is critical to the degeneration and regeneration processes. These findings suggest that the activation of MK after nerve injury plays a beneficial role in nerve regeneration.

ACKNOWLEDGMENTS

We greatly appreciate the advice and assistance of Dr. Mistuo Anraku, Kagoshima University.

REFERENCES

Blondet B, Carpentier G, Lafdil F, Courty J. 2005. Pleiotrophin cellular location in nerve regeneration after peripheral nerve injury. J Histochem Cytochem 53:971–977.

Blondet B, Carpentier G, Ferry A, Courty J. 2006. Exogenous pleiotrophin applied to lesioned nerve impairs muscle reinnervation. Neurochem Res 31:907–913.

Ezquerra L, Alguacil LF, Nguyen T, Deuel TF, Silos-Santiago I, Herradon G. 2008. Different pattern of pleiotrophin and midkine expression in neuropathic pain: correlation between changes in pleiotrophin gene expression and rat strain differences in neuropathic pain. Growth Factors 26:44–48.

Gao WQ, Shinsky N, Ingle G, Beck K, Elias KA, Powell-Braxton L. 1999. IGF-1 deficient mice show reduced peripheral nerve conduction velocities and decreased axonal diameters and respond to exogenous IGF-1 treatment. J Neurobiol 39:142–152.

Huang RP, Muramatsu H, Muramatsu T. 1990. Effects of different conditions of retinoic acid treatment on expression of MK gene, which is transiently activated during differentiation of embryonal carcinoma cells. Dev Growth Differ 32:280–289.

Ide C. 1996. Peripheral nerve regeneration. Neurosci Res 25:101–121.

Igakura T, Kadomatsu K, Kaname T, Muramatsu H, Fan QW, Miyauchi T, Toyama Y, Kuno N, Yuasa S, Takahashi M, Senda T, Taguchi O, Yamamura K, Arimura K, Muramatsu T. 1998. A null mutation in basigin, an immunoglobulin superfamily menber, indicates its important roles in peri-implantation development and spermatogenesis. Dev Biol 194:152–165.

Inserra MM, Yao M, Murray R, Terris DJ. 2000. Peripheral nerve regeneration in interleukin 6-deficient mice. Arch Otolaryngol Head Neck Surg 126:1112–1116.

Jiang Y, Mclennan IS, Koishi K, Hendry IA. 2000. Transforming growth factor-beta 2 is anteogradely and retrogradely transported in motoneurons and up-regulated after nerve injury. Neuroscience 97:735–742.

Kadomatsu K, Tomomura M, Muramatsu T. 1988. cDNA cloning and sequencing of a new gene intensely expressed in early differentiation stages of embryonal carcinoma cells and in mid-gestation period of mouse embryogenesis. Biochem Biophys Res Commun 151:1312–1318.

Kadomatsu K, Huang RP, Suganuma T, Murata F, Muramatsu T. 1990. A retinoic acid responsive gene MK found in the teratocarcinoma system is expressed in spatially and temporally controlled manner during mouse embrogenesis. J Cell Biol 110:607–616.

Keilhoff G, Fansa H, Wolf G. 2002. Difference in peripheral nerve degeneration/regeneration between wild type and neuronal nitric oxide synthase knockout mice. J Neurosci Res 68:432–441.

Kosugi T, Yuzawa Y, Sato W, Arata-Kawai H, Suzuki N, Kato N, Matsuo S, Kadomatsu K. 2007. Midkine is involved in tubulointerstitial inflammation associated with diabetic nephropathy. Lab Invest 87:903–913.

Maruyama K, Muramatsu H, Ishiguro N, Muramatsu T. 2004. Midkine, a heparin-binding growth factor, is fundamentally involved in the pathogenesis of rheumatoid arthritis. Arthritis Rheum 50:1420–1429.

Mclean J, Batt J, Doering LC, Rotin D, Bain JR. 2002. Enhanced rate of nerve regeneration and directional errors after sciatic nerve injury in receptor protein tyrosine phoshatase ó knock-out mice. J Neurosci 22:5481–5491.

Michikawa M, Kikuchi S, Muramatsu H, Muramatsu T, Kim SU. 1992. Retinoic acid responsive gene product, midkine (MK), has neurotrophic functions for mouse spinal cord and dorsal root ganglion neurons in culture. J Neurosci Res 35:530–539.

Muramatsu H, Shirahama H, Yonezawa S, Maruta H, Muramatsu T. 1993. Midkine, a retinoic acid-inducible growth/differentiation factor: immunochmical evidence for the function and distribution. Dev Biol 159:392–402.

Muramatsu T. 2002. Midkine and pleiotrophin: tworelated proteins involved in development, survival, inflammation and tumorigenesis. J Biochem 132:359–371.

Nakamura E, Kadomatsu K, Yuasa S, Muramatsu H, Mamiya T, Nabeshima T, Fan QW, Ishiguro K, Igakura T, Matsubara S, Kaname T, Horiba M, Saito H, Muramatsu T. 1998. Disruption of the midkine gene (Mdk) resulted in altered expression of a calcium binding protein in the hippocampus of infant mice and their abnormal behaviour. Genes Cells 3:811–822.

Ohta S, Muramatsu H, Senda T, Zou K, Iwata H, Muramatsu T. 1999. Midkine is expressed during repair of bone fracture and promotes chondrogenesis. J Bone Miner Res 14:1132–1144.

Reichert F, Saada A, Rptshenker S. 1994. Peripheral nerve injury induces schwann cells to express two macrophage phenotype: phagocytosis and the galactose-specific lectin MAC-2. J Neurosci 14:3231–3245.

Sakakima H, Kawamata S, Kai S, Ozawa J, Matuura N. 2000. Effects of short-term denervation and subsequent reinnervation on motor endplate and the soleus muscle in the rat. Arch Histol Cytol 63:495–506.

Sakakima H, Yoshida Y, Muramatsu T, Yone K, Goto M, Ijiri K, Izumo S. 2004a. Traumatic injury-induced midkine expression in the adult rat spinal cord during the early stage. J Neurotrauma 41:471–477.

Sakakima H, Yoshida Y, Kadomatsu K, Yuzawa Y, Matsuo S, Muramatsu T. 2004b. Midkine expression in rat spinal motor neurons following sciatic nerve injury. Brain Res Dev Brain Res 153:251–260.

Sakakima H, Kamizono T, Matsuda F, Izumo K, Yoshida Y. 2006. Midkine and its receptor in regenerating rat skeletal muscle after bupivacaine injection. Acta Histchem 108:357–364.

Sato W, Kadomatsu K, Yuzawa Y, Muramatsu H, Hotta N, Matsuo S, Muramatsu T. 2001. Midkine is involved in neutrophill infiltration into the tubulointerstitium in ischemic renal injury. J Immunol 167: 3463–3469.

Takada T, Toriyama K, Muramatsu H, Song XJ, Torii S, Muramatsu T. 1997. Midkine, a retinoic acid-inducible heparin-binding cytokine in inflammatory responses: chemotactic activity to neutrophils and association with inflammatory synovitis. J Biochem 122:453–458.

Tsutsui J, Kadomatsu K, Matsubara S, Nakagawara A, Hamanoue M, Takao S, Shimazu H, Ohi Y, Muramatsu T. 1993. A new family of heparin-binding growth/differentiation factors: increased midkine expression in Wilms' tumor and other human carcinomas. Cancer Res 53:1281–1285.

Wada M, Kamata M, Aizu Y, Morita T, Hu J, Oyanagi K. 2002. Alteration of midkine expression in the ischemic brain in human. J Neurol Sci 200:67–73.

Yamamoto M, Sobue G, Li M, Arakawa Y, Mitsuma T, Kimata K. 1993. Nerve growth factor (NGF), brain-derived neurotrophic factor (BDNF) and low-affinity nerve growth factor receptor (LNGFR) mRNA levels in cultured rat Schwann cells: differential time-and dose-dependent regulation by cAMP. Neurosci Lett 152:37–40.

Yao M, Moir MS, Wang MZ, To MP, Terris DJ. 1999. Peripheral nerve regeneration in CNTF knockout mice. Laryngoscope 109:1263–1268.

Yasuhara H, Muramatsu H, Kim SU, Muramatsu T, Maruta H, MgGeer PL. 1993. Midkine, a novel neurotrophic factor, is present in senile plaques of Alzheimer disease. Biochem Biophys Res Commun 192: 3545–3550.

Yoshida Y, Goto M, Tsutsui J, Ozawa M, Sato E, Osame M, Muramatu T. 1995. Midkine is present in the early stage of cerebral infarct. Brain Res Dev Brain Res 85:25–30.

Yoshida Y, Ikematsu S, Moritoyo T, Goto M, Tsutsui J, Sakuma S, Osame M, Muramatsu T. 2001. Intraventricular administration of the neurotorophic factor midkine ameliorates hippocampal delay neuronal death following transient forebrain ischemia in gerbils. Brain Res 894:46–55.

The growth factor midkine regulates the renin-angiotensin system in mice

Akinori Hobo,[1,2] Yukio Yuzawa,[2] Tomoki Kosugi,[2] Noritoshi Kato,[1,2] Naoto Asai,[2] Waichi Sato,[2] Shoichi Maruyama,[2] Yasuhiko Ito,[2] Hiroyuki Kobori,[3] Shinya Ikematsu,[4] Akira Nishiyama,[5] Seiichi Matsuo,[2] and Kenji Kadomatsu[1]

[1]Department of Biochemistry and [2]Department of Nephrology, Nagoya University Graduate School of Medicine, Nagoya, Japan.
[3]Department of Physiology and Hypertension & Renal Center of Excellence, Tulane University Health Sciences Center, New Orleans, Louisiana, USA.
[4]Department of Bioresources Engineering, Okinawa National College of Technology, Okinawa, Japan.
[5]Department of Pharmacology and Hypertension & Kidney Disease Research Center, Kagawa University Medical School, Kagawa, Japan.

The renin-angiotensin system plays a pivotal role in regulating blood pressure and is involved in the pathogenesis of kidney disorders and other diseases. Here, we report that the growth factor midkine is what we believe to be a novel regulator of the renin-angiotensin system. The hypertension induced in mice by 5/6 nephrectomy was accompanied by renal damage and elevated plasma angiotensin II levels and was ameliorated by an angiotensin-converting enzyme (ACE) inhibitor and an angiotensin receptor blocker. Notably, ACE activity in the lung, midkine expression in the lung, and midkine levels in the plasma were all increased after 5/6 nephrectomy. Exposure to midkine protein enhanced ACE expression in primary cultured human lung microvascular endothelial cells. Furthermore, hypertension was not induced and renal damage was less severe in midkine-deficient mice. Supplemental administration of midkine protein to midkine-deficient mice restored ACE expression in the lung and hypertension after 5/6 nephrectomy. Oxidative stress might be involved in midkine expression, since expression of NADH/NADPH oxidase–1, –2, and –4 was induced in the lung after 5/6 nephrectomy. Indeed, the antioxidative reagent tempol reduced midkine expression and plasma angiotensin II levels and consequently ameliorated hypertension. These results suggest that midkine regulates the renin-angiotensin system and mediates the kidney-lung interaction after 5/6 nephrectomy.

Introduction

The renin-angiotensin system (RAS) is a hormonal cascade that functions in the homeostatic control of arterial pressure, tissue perfusion, and extracellular volume. Dysregulation of the RAS results in the pathogenesis of many diseases, including cardiovascular and renal disorders (1–3). The RAS is initiated by the regulated secretion of renin, which catalyzes the hydrolysis of Ang I from the N terminus of angiotensinogen. Ang I is in turn hydrolyzed by angiotensin-converting enzyme (ACE) to form Ang II, the primary active product of the RAS (4, 5). ACE is a zinc metallopeptidase widely distributed on the cell membrane of endothelial and epithelial cells (6). Ang II induces vasoconstriction and aldosterone release, leading to upregulation of blood pressure. It also exerts its vasoconstrictor effect on both the afferent and efferent arterioles, which may contribute to the onset and progression of chronic renal damage. Ang II may also directly contribute to the acceleration of renal damage by sustaining cell growth, inflammation, and fibrosis (7).

The growth factor midkine (MK; gene symbol, *MDK*) is implicated in cancer progression, neuronal survival and differentiation, and inflammation (8). MK is involved in the pathogeneses of tubulointerstitial damage induced by renal reperfusion and glomerular sclerosis associated with diabetes mellitus (9, 10). The finding of a recent report that angiotensinogen and renin expression was significantly elevated in the aorta of $Mdk^{-/-}$ mice while ACE expression was significantly suppressed is of particular interest (11). However, $Mdk^{-/-}$ mice develop normally (8), and there has been no report of systemic disturbance or organ disorders of $Mdk^{-/-}$ mice. Therefore, the biological meaning of changes in the RAS molecules in the aorta of $Mdk^{-/-}$ mice has remained obscure.

It is widely accepted that the RAS is involved in the pathogenesis of chronic kidney disease (CKD), and inhibitors of the RAS are the first choice of therapy for CKD (12–14). To investigate the molecular mechanisms regulating the RAS in CKD, we employed 5/6 nephrectomy in this study. 5/6 nephrectomized mice are a popular and useful model of CKD, since the remnant kidney model of progressive renal injury is characterized by systemic hypertension and glomerular hyperfiltration, the latter eventually causing glomerular sclerosis (15, 16). CKD accompanies multiple organ failure, the pathogenesis of which involves inter-organ cross-talk (17, 18). In this context, it is noteworthy that MK expression was induced in the lung by 5/6 nephrectomy, leading to elevation of ACE activity and plasma Ang II levels and subsequent hypertension in the present study. Our data therefore suggest that MK is a candidate mediator of inter-organ cross-talk in CKD.

Results

MK is involved in RAS activation induced by 5/6 nephrectomy. Systolic and mean blood pressure were comparable in untreated $Mdk^{+/+}$ and $Mdk^{-/-}$ mice (Figure 1, A and B). However, we found that 5/6 nephrectomy strikingly increased blood pressure in $Mdk^{+/+}$ mice but not in $Mdk^{-/-}$ mice (Figure 1, A and B). The systolic and mean blood pressure of $Mdk^{+/+}$ mice strikingly increased after 2 weeks, but $Mdk^{-/-}$ mice showed almost normal blood pressure, i.e., no

Conflict of interest: The authors have declared that no conflict interest exists.

Nonstandard abbreviations used: ACE, angiotensin-converting enzyme; BIS, bisindolylmaleimide I; CKD, chronic kidney disease; HMVEC-L, human lung microvascular endothelial cell(s); MK, midkine; Nox, NADPH oxidase; PTN, pleiotrophin; RAS, renin-angiotensin system; rh-MK, recombinant human MK.

Citation for this article: *J. Clin. Invest.* **119**:1616–1625 (2009). doi:10.1172/JCI37249.

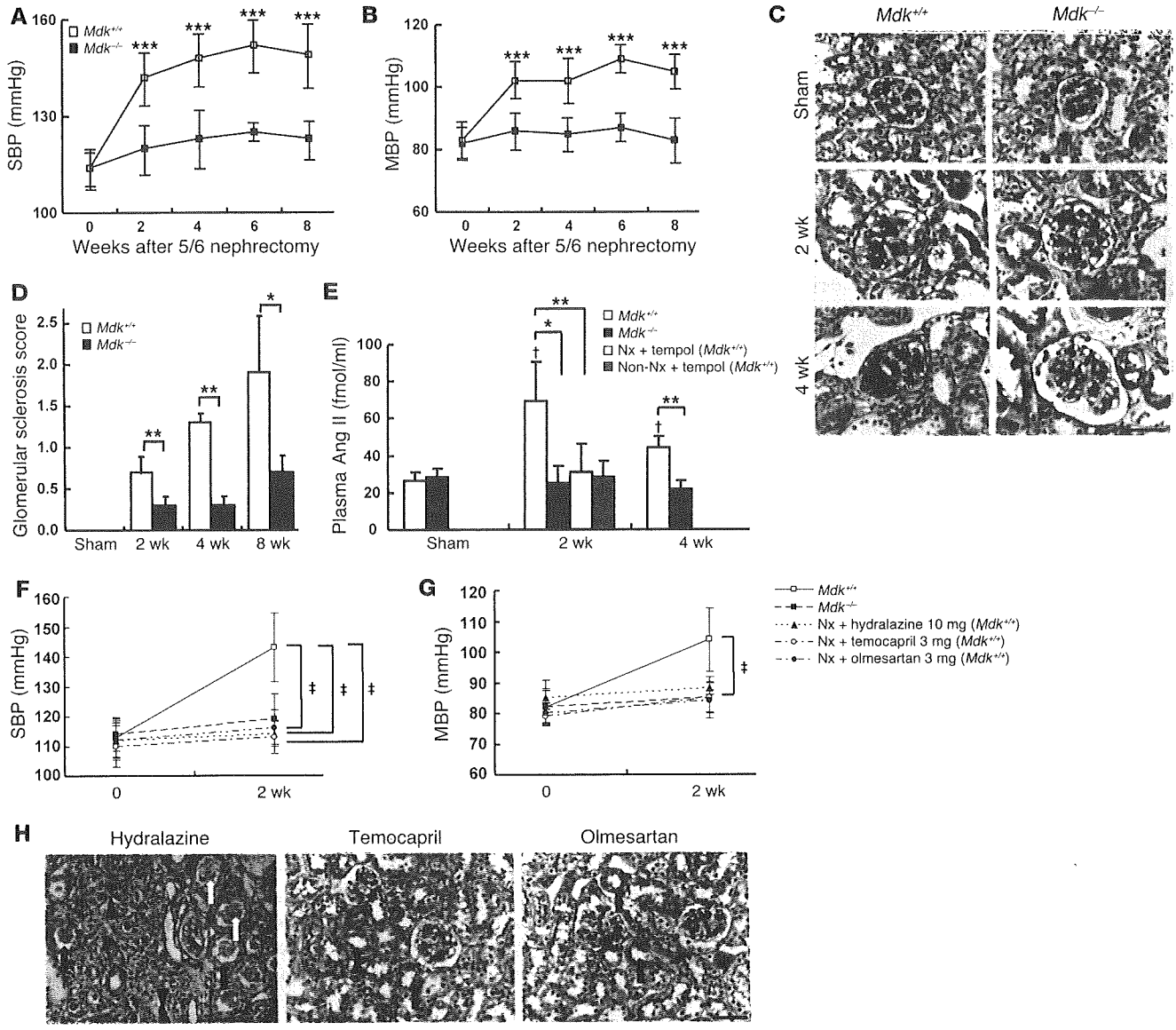

Figure 1

5/6 nephrectomy induces hypertension and renal damage via the RAS. (**A** and **B**) Blood pressure was measured at 0, 2, 4, 6, and 8 weeks after 5/6 nephrectomy. Systolic blood pressure (SBP) (**A**) and mean blood pressure (MBP) (**B**) were measured by the tail-cuff method. The mean and SD are represented by squares and bars, respectively, at each time point ($Mdk^{+/+}$: 0 weeks, n = 40; 2 weeks, n = 34; 4 weeks, n = 19; 8 weeks, n = 8; $Mdk^{-/-}$: 0 weeks, n = 26; 2 weeks, n = 23; 4 weeks, n = 13; 8 weeks, n = 4). ***$P < 0.001$ versus $Mdk^{-/-}$ mice. (**C**) Representative glomerular histology shown by PAS staining. Scale bar: 50 μm. (**D**) Semiquantitative analysis of the glomerular sclerosis score. Data are shown as mean and SD ($Mdk^{+/+}$: 2 weeks, n = 5; 4 weeks, n = 4; 8 weeks, n = 4; $Mdk^{-/-}$: 2 weeks, n = 4; 4 weeks, n = 3; 8 weeks, n = 3). (**E**) Plasma Ang II concentration after 5/6 nephrectomy ($Mdk^{+/+}$: sham, n = 6; 2 weeks, n = 6; 4 weeks, n = 8; $Mdk^{-/-}$: sham, n = 6; 2 weeks, n = 7; 4 weeks, n = 5). *$P < 0.05$, **$P < 0.01$; †$P < 0.01$ versus sham $Mdk^{+/+}$. Nx, nephrectomy. (**F** and **G**) Effects of hydralazine, temocapril, and olmesartan on blood pressure. SBP (**F**) and MBP (**G**) were measured by the tail-cuff method (n = 3). ‡$P < 0.01$ versus $Mdk^{+/+}$ mice. (**H**) Representative histology after treatment with hydralazine, temocapril, and olmesartan. The kidney specimens were stained with PAS. Tubular dilatation (black arrows), tubular cast formation (arrowheads), and tubular degeneration (white arrows) are indicated. Scale bar: 50 μm.

significant increase (systolic blood pressure, 143 ± 11.6 mmHg in $Mdk^{+/+}$ mice vs. 119 ± 8.6 mmHg in $Mdk^{-/-}$ mice; mean blood pressure, 104 ± 10.3 mmHg vs. 85 ± 6.7 mmHg). Consequently, systolic and mean blood pressures were significantly higher in $Mdk^{+/+}$ than in $Mdk^{-/-}$ mice from 2 to 8 weeks (Figure 1, A and B).

5/6 nephrectomy caused not only hypertension but also progressive renal failure. Blood urea nitrogen and serum creatinine levels gradually increased, and both parameters were significantly higher in $Mdk^{+/+}$ mice at 2 and 4 weeks after renal ablation (Table 1). $Mdk^{+/+}$ mice also exhibited more severe glomerular sclerosis, which is characterized by a marked deposition of extracellular matrix in the glomeruli and which occurred as early as 2 weeks after renal ablation (Figure 1C). Semiquantitative analysis of the glomerular sclerosis scores revealed significant differences between $Mdk^{+/+}$

Table 1
Body weight, blood urea nitrogen, serum creatinine, and left kidney weight after 5/6 nephrectomy

	BW (g)	BUN (mg/dl)	Cre (mg/dl)	Left kidney wt (mg)
Before nephrectomy				
Mdk$^{+/+}$	22.2 ± 2.1	21.2 ± 3.7	0.06 ± 0.02	–
Mdk$^{-/-}$	21.3 ± 1.3	19.7 ± 1.4	0.04 ± 0.02	–
Hydralazine, 10 mg/kg/d	23.1 ± 0.6	ND	ND	–
Temocapril, 3 mg/kg/d	22.0 ± 2.0	ND	ND	–
Olmesartan, 3 mg/kg/d	24.5 ± 0.5	ND	ND	–
Tempol, 3 mmol/l	22.7 ± 1.7	ND	ND	–
2 weeks after nephrectomy				
Mdk$^{+/+}$	19.7 ± 2.2	57.1 ± 9.7	0.65 ± 0.11	104.8 ± 9.6
Mdk$^{-/-}$	18.8 ± 1.5	39.5 ± 7.2^{A}	0.39 ± 0.08^{A}	104.3 ± 15.1
Hydralazine, 10 mg/kg/d	18.7 ± 0.7	63.3 ± 7.6	0.53 ± 0.12	ND
Temocapril, 3 mg/kg/d	19.7 ± 2.7	30.3 ± 2.9^{A}	0.21 ± 0.04^{A}	ND
Olmesartan, 3 mg/kg/d	21.3 ± 0.7	36.0 ± 1.0^{B}	0.21 ± 0.01^{A}	ND
Tempol, 3 mmol/l	21.4 ± 1.6	41.2 ± 3.9^{B}	0.25 ± 0.04^{A}	ND
4 weeks after nephrectomy				
Mdk$^{+/+}$	20.9 ± 1.8	66.1 ± 8.7	0.77 ± 0.13	130.0 ± 21.4
Mdk$^{-/-}$	20.6 ± 1.7	46.4 ± 4.8^{A}	0.44 ± 0.15^{B}	130.3 ± 10.7
8 weeks after nephrectomy				
Mdk$^{+/+}$	22.5 ± 1.9	71.9 ± 14.6	1.56 ± 0.34	118.5 ± 14.9
Mdk$^{-/-}$	21.2 ± 2.3	62.9 ± 12.9	1.18 ± 0.29	128.5 ± 6.0

Values are mean ± SD. BUN, blood urea nitrogen; Cre, serum creatinine. ND, no data. Hydralazine, temocapril, olmesartan, and tempol were administered to *Mdk*$^{+/+}$ mice at the indicated doses. $^{A}P < 0.001$ versus *Mdk*$^{+/+}$. $^{B}P < 0.01$ versus *Mdk*$^{+/+}$.

and *Mdk*$^{-/-}$ mice (Figure 1D). In addition, the tubulointerstitial damage was worse in *Mdk*$^{+/+}$ mice (Supplemental Figure 1; supplemental material available online with this article; doi:10.1172/JCI37249DS1). Thus, tubular dilatation, cast formation in the tubular lumen, and tubular epithelial degeneration became apparent at 2 weeks after renal ablation and were more severe in *Mdk*$^{+/+}$ mice (Supplemental Figure 1, A–H). Interstitial fibrosis, as evidenced by collagen deposition revealed by Masson's trichrome staining, was exhibited at 4 weeks and then more diffusely at 8 weeks, and the stained area became expanded in *Mdk*$^{+/+}$ mice (Supplemental Figure 1, I–P). These data collectively indicate that renal damage was more severe in *Mdk*$^{+/+}$ mice than in *Mdk*$^{-/-}$ mice.

These symptoms of hypertension and renal damage were attributable to the RAS, as (a) the hypertension was accompanied by elevated plasma Ang II concentration (Figure 1E); and (b) the ACE inhibitor temocapril and the angiotensin receptor blocker olmesartan reduced both blood pressure and renal tubulointerstitial damage, but the vasodilator hydralazine only ameliorated hypertension (Figure 1, F–H). Abnormal elevation of blood urea nitrogen and serum creatinine was ameliorated by administration of temocapril and olmesartan, but not hydralazine (Table 1). It is therefore conceivable that the RAS contributed to both hypertension and renal damage.

ACE levels are increased in the lung after 5/6 nephrectomy. Expression of the intrarenal angiotensinogen and renin was suppressed and ACE expression was unchanged in *Mdk*$^{+/+}$ mice, which was consistent with previous findings after 5/6 nephrectomy of rats (19, 20) (Supplemental Figure 2, A–C). In contrast to the kidney, the lung showed significant increases in ACE expression and its activity 2 and 4 weeks after renal ablation (Figure 2, A–E). ACE protein expression was localized to the pulmonary vascular endothelial cells and alveolar-capillary endothelial cells, consistent with a previous report (Figure 2D) (21).

Other organs that play major functions in the RAS were also examined for their expression of RAS components. Angiotensinogen mRNA expression was induced in the liver after 5/6 nephrectomy, but the expression level was not significantly different in *Mdk*$^{+/+}$ and *Mdk*$^{-/-}$ mice (Supplemental Figure 3A). There was no difference in angiotensinogen protein levels between the two genotypes (Supplemental Figure 3, B and C), and renin mRNA expression was not detected in the liver (data not shown). Expression of ACE protein and MK protein was also not detected in the liver (Supplemental Figure 3, D and E). In the brain, mRNA expression of angiotensinogen and ACE did not change after 5/6 nephrectomy (Supplemental Figure 4, A and B), and the renin mRNA expression was undetectable (data not shown). ACE protein was also not detected in the brain (Supplemental Figure 4C). Furthermore, the mRNA expression of angiotensinogen, renin, and ACE did not change in the heart (Supplemental Figure 5). Therefore, it is most likely that the hypertension observed after 5/6 nephrectomy was due to activation of the lung ACE.

MK levels are increased in the lung, kidney, and plasma after 5/6 nephrectomy. MK expression was increased in the lung in association with an elevation in ACE expression (Figure 3, A–C). MK protein was localized to the endothelium of microvessels of the lung, as revealed by the use of thrombomodulin as a marker of the vascular endothelium (Figure 3D). MK expression was detected in alveolar-capillary endothelial cells but not in bronchial epithelial cells (Figure 3D).

Histological evidence of lung damage, i.e., due to edema and degeneration of alveolar cells, was not observed after 5/6 nephrectomy in the *Mdk*$^{+/+}$ and *Mdk*$^{-/-}$ mice (Supplemental Figure 6A). Increases in macrophage and neutrophil infiltration into the lung were also not observed after 5/6 nephrectomy in the two genotypes (Supplemental Figure 6, B–E). These results indicated that the increase in MK expression in the lung after 5/6 nephrectomy was not due to leukocytes.

MK expression was also significantly elevated in the kidney at both the protein and mRNA levels 2 and 4 weeks after renal ablation (Supplemental Figure 7, A–C). Immunohistochemical analysis revealed that MK protein was mainly localized in the tubular epithelium (Supplemental Figure 8A). This result is consistent with previous reports in which MK was expressed in the kidney after ischemia/reperfusion injury and its associated massive leukocyte infiltration (22). We also detected a substantial increase in macrophage infiltration into the kidney after 5/6 nephrectomy, and this increase was significantly higher in *Mdk*$^{+/+}$ mice than *Mdk*$^{-/-}$ mice (Supplemental Figure 8, B and C). It is known that MK is expressed by activated macrophages (23, 24). Thus, it is conceivable that the increase in MK expression in the kidney after 5/6 nephrectomy was due to enhanced expression in both the tubular epithelium and infiltrating macrophages.

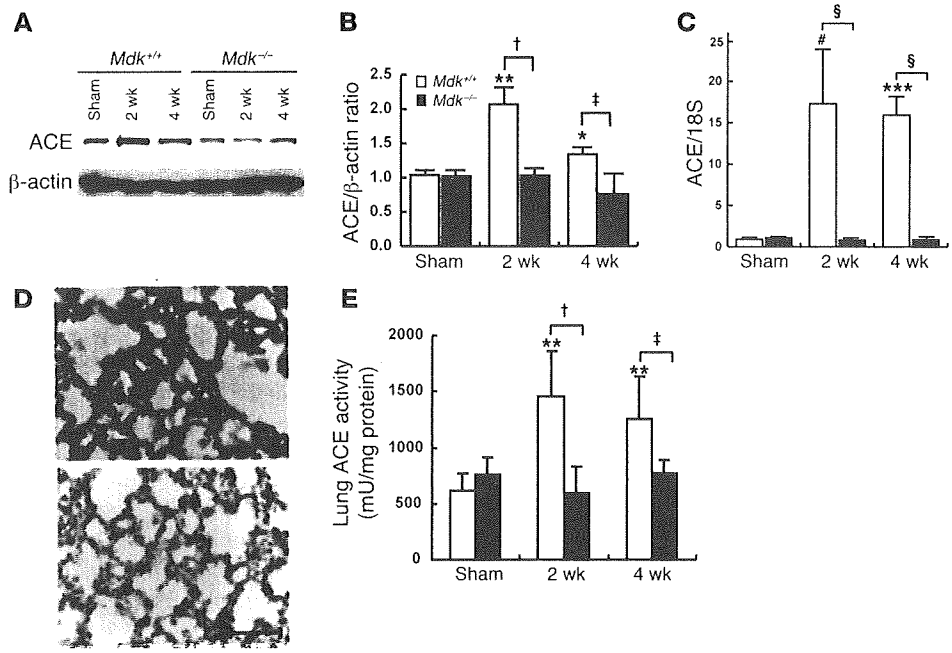

Figure 2

ACE expression in the lung after 5/6 nephrectomy. (**A**) ACE protein was determined by Western blotting, and a representative result is shown. The lung tissues were obtained at the indicated time points. (**B**) Quantitative analysis of ACE protein expression using densitometry. Data are presented as mean and SD (n = 3). $^{\dagger}P < 0.01$; $^{\ddagger}P < 0.05$; $^{*}P < 0.05$ and $^{**}P < 0.01$ versus sham *Mdk*$^{+/+}$. (**C**) ACE mRNA was determined by real-time PCR and normalized to 18S mRNA. Data are presented as mean and SD (*Mdk*$^{+/+}$: sham, n = 5; 2 weeks, n = 5; 4 weeks, n = 3; *Mdk*$^{-/-}$: sham, n = 3; 2 weeks, n = 3; 4 weeks, n = 3). $^{\S}P < 0.0001$; $^{***}P < 0.001$ and $^{\#}P < 0.0001$ versus sham *Mdk*$^{+/+}$. (**D**) Immunohistochemical staining of lungs with mouse anti-ACE monoclonal antibody at 2 weeks. Upper panel: The first antibody used was anti–mouse ACE monoclonal antibody. Lower panel: Isotype-matched IgG was used as the first antibody. Scale bar: 50 μm. (**E**) ACE activity was determined by the ACE activity assay, as described in Methods. Data are presented as mean and SD (*Mdk*$^{+/+}$: sham, n = 5; 2 weeks, n = 5; 4 weeks, n = 5; *Mdk*$^{-/-}$: sham, n = 5; 2 weeks, n = 5; 4 weeks, n = 4). $^{\dagger}P < 0.01$; $^{\ddagger}P < 0.05$; $^{**}P < 0.01$ versus sham *Mdk*$^{+/+}$.

Since MK is a secreted protein, and its expression was induced by 5/6 nephrectomy in the kidney and lung (Figure 3, A–C, and Supplemental Figure 7, A–C), we next examined plasma MK levels. As shown in Figure 3, E and F, plasma MK levels were indeed increased 2 weeks after 5/6 nephrectomy.

Exogenous MK induces ACE expression. If MK is required for ACE expression in the lung and hypertension, supplementary administration of MK might also affect these symptoms. To clarify this issue, we administered exogenous MK continuously through an osmotic pump into *Mdk*$^{-/-}$ mice after 5/6 nephrectomy. This administration was found to restore hypertension and ACE expression in the lung (Figure 4, A–C). We also administered pleiotrophin (PTN; also called HB-GAM), which shows 50% homology with MK (8), to *Mdk*$^{-/-}$ mice after 5/6 nephrectomy. However, exogenous PTN neither induced hypertension nor increased ACE expression in the lung (Figure 4, A, D, and E). These data support the specificity of MK with respect to its involvement in ACE expression and blood pressure regulation.

Furthermore, exogenous MK protein on primary cultured human lung microvascular endothelial cells (HMVEC-L) significantly enhanced ACE expression, suggesting that ACE is one of the targets of MK in the lung (Figure 5, A and B). When Ang I was added to the culture medium of the lung endothelial cells treated with MK and heparin for 36 hours, Ang I was converted to Ang II in a time-dependent manner, while cells treated with heparin alone did not show such a conversion (Figure 5C). These results suggest that MK is a potent inducer of Ang II through upregulation of ACE expression in lung endothelial cells.

Along with the increase in ACE expression, phosphorylation levels of PKC were also increased in primary cultured HMVEC-L after exposure to exogenous MK (Figure 5, D and E). This result suggests that MK upregulates ACE expression through activation of PKC. This idea was further supported by three lines of evidence. First, bisindolylmaleimide I (BIS), a PKC-specific inhibitor, blocked the MK-mediated increase in ACE expression (Figure 5, A and B). Second, PKC phosphorylation was significantly increased in the lungs of *Mdk*$^{+/+}$ but not *Mdk*$^{-/-}$ mice after 5/6 nephrectomy (Figure 5F). Third, consistent with previous reports (25), the increase in ACE expression in primary cultured HMVEC-L was also induced by PMA, a PKC activator, and was blocked by BIS (Supplemental Figure 9).

Oxidant stress induces MK expression in the lung after 5/6 nephrectomy. Finally, the mechanism of MK induction in the lung by 5/6 nephrectomy was investigated. The NADPH oxidases (Nox's) are superoxide-generating enzymes that release superoxide by electron transfer from NADPH to oxygen. Increased production of ROS has been implicated in various pathologies, including hypertension, atherosclerosis, diabetes, and CKD (26, 27). In the present study, Nox1, -2, and -4 mRNA expression in the lungs of *Mdk*$^{+/+}$ mice was found to be significantly increased at 2 and 4 weeks after renal ablation compared with the levels in the sham-operated animals, suggesting that oxidant stress was generated in the lung; in contrast, the expression of Nox1, -2, and -4 mRNA was unchanged in the *Mdk*$^{-/-}$ mice (Figure 6A). A cell membrane–permeable radical scavenger, 4-hydroxy-2,2,6,6-tetramethylpiperidine-*N*-oxyl (tempol), reduced MK expression to normal levels in the lung (Figure 6B); plasma Ang II levels (Figure 1E) and blood pressure (Figure 6C) were also reduced. Tempol also ameliorated glomerular sclerosis and tubulointerstitial damage (Figure 6D) and improved renal function, i.e., significantly reduced blood urea nitrogen and serum creatinine levels (Table 1). These results suggest that MK expression was induced by oxidative stress in the lung after 5/6 nephrectomy. Tempol also reduced MK expression in the kidney (Supplemental Figure 7, D and E).

Discussion

Our study demonstrated that *Mdk*$^{-/-}$ mice had almost normal blood pressure after 5/6 nephrectomy, while wild-type mice showed

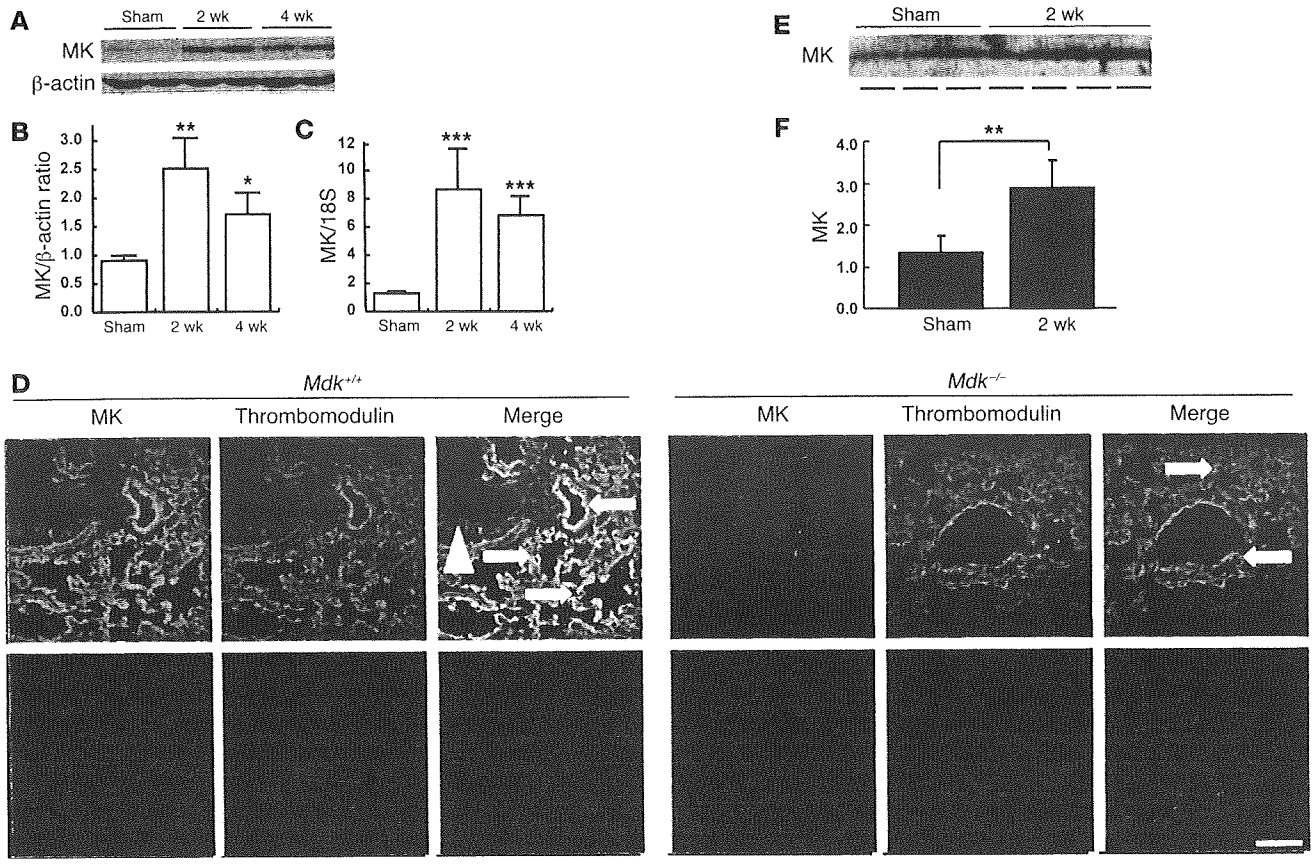

Figure 3

MK expression in the lung and plasma after 5/6 nephrectomy. (**A**) Representative data from Western blotting for MK expression in the lung. (**B**) The intensity of MK bands on Western blotting was normalized to that of β-actin. Data are presented as mean and SD ($n = 4$). $^{*}P < 0.05$ and $^{**}P < 0.01$ versus sham. (**C**) MK mRNA expression in the lung was determined by real-time PCR and normalized to 18S mRNA. Data are presented as mean and SD (sham, $n = 5$; 2 weeks, $n = 5$; 4 weeks, $n = 3$). $^{***}P < 0.001$ versus sham. (**D**) Immunofluorescence staining of MK and thrombomodulin expression in the lung 2 weeks after 5/6 nephrectomy. Lower panels show negative controls using isotype-matched IgG as the first antibody. Arrowhead, bronchial epithelial cells; white arrows, alveolar-capillary endothelial cells. Scale bar: 50 μm. (**E**) Representative data from Western blotting for MK expression in plasma are shown. Lines under the blot indicate individual samples. (**F**) Western blot data for plasma MK were quantified using densitometry and are presented as mean and SD (sham, $n = 4$; 2 weeks, $n = 5$). $^{**}P < 0.01$.

marked hypertension. This hypertension was ameliorated by RAS-related inhibitors and indeed was accompanied by elevated plasma Ang II levels. Surprisingly, ACE activity was enhanced in the lung, whereas RAS components were not activated in other organs. Plasma MK levels and MK expression in the lung and kidney were elevated. Supplementary MK administration to *Mdk*$^{-/-}$ mice restored lung ACE expression and hypertension. MK also induced ACE expression and consequently conversion from Ang I to Ang II in primary cultured lung microvascular endothelial cells. We therefore concluded that MK-mediated ACE induction in the lung is critical for hypertension induced by 5/6 nephrectomy (Figure 7).

Inter-organ interactions involving the kidney have recently been highlighted. Regarding factors affecting lung function after acute kidney injury, several cytokines, including IL-6, IL-1β, and TNF-α, have been suggested as candidates (28, 29). Such results contribute to our understanding of the high mortality associated with pulmonary complications following acute kidney injury. CKD has also been linked with damage in other organs, especially with cardiovascular damage (so-called cardiorenal syndrome) (30). It is particularly interesting that RAS components are increased in the heart and brain of subtotally nephrectomized rats (20, 31) and that Ang II amounts are increased in the isolated perfused hind limbs of uremic rats (32). Inhibitors of the RAS, e.g., angiotensin receptor blockers and ACE inhibitors, are indeed the first choice of therapy for CKD (33). Our results clearly show that the lung is a promising target in the cross-talk between the kidney and other organs and suggest that MK is a candidate mediator for pulmonary and other organ complications associated with CKD.

Regarding the cross-talk between the kidney and lung in 5/6 nephrectomy, our study has also provided an insight into the underlying mechanism. We found that Nox1, -2, and -4 were induced in the lung and that tempol reduced MK and plasma Ang II levels. Nox mediates the initial reaction of 3 successive reduction products of molecular oxygen, i.e., superoxide ($O_2^{\bullet-}$), hydrogen peroxide (H_2O_2), and hydroxyl radical ($OH^{\bullet}$). Since tempol is a membrane-permeable and metal-independent superoxide dismutase mimetic that is specific for superoxide anion ($O_2^{\bullet-}$) (34, 35), tempol may target ROS initiated by Nox in the lung. To the best of our knowledge, this is the first study to show that 5/6 nephrectomy induces oxidative stress in the lung. We have previously reported that oxidative

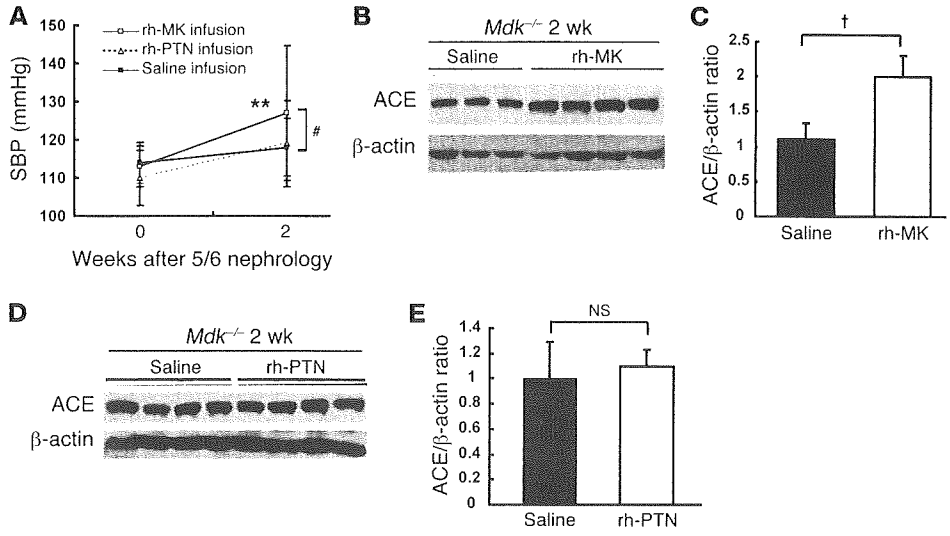

Figure 4
Effects of exogenous MK and PTN in *Mdk*$^{-/-}$ mice on blood pressure and ACE expression in the lung. (**A**) SBP was measured by the tail-cuff method at 0 and 2 weeks after 5/6 nephrectomy (n = 5). $^{**}P < 0.01$ versus untreated *Mdk*$^{-/-}$ mice (0 weeks); $^{\#}P < 0.01$, rh-MK versus saline. rh-PTN, recombinant human PTN. (**B**) ACE expression in the lung of *Mdk*$^{-/-}$ mice treated with MK and saline. Western blot data are shown. (**C**) The data in **B** were quantified using densitometry and are presented as mean and SD. $^{\dagger}P < 0.01$. (**D**) ACE expression in the lung of *Mdk*$^{-/-}$ mice treated with rh-PTN and saline. Western blot data are shown. (**E**) The data in **D** were quantified using densitometry and are presented as mean and SD.

stress induces MK expression (10, 22). Therefore, it is conceivable that Nox-mediated ROS production leads to an induction of MK expression in the lung (Figure 7). As ROS have very short half-lives (36), it is not likely that the ROS themselves travel between the kidney and lung. Furthermore, it is widely accepted that Ang II induces Nox expression (37). Based on this background data, we speculate that the following molecular circuit is established after circulating MK induces ACE expression in the lung: Ang II induces Nox expression, which in turn initiates ROS production and subsequently MK and ACE expression (Figure 7).

RAS-related inhibitors, but not hydralazine, ameliorated renal damage in the present study. It has also been reported that systemically administered Ang II worsens renal function (38–40). Therefore, the RAS might play at least a partial role in renal damage. In

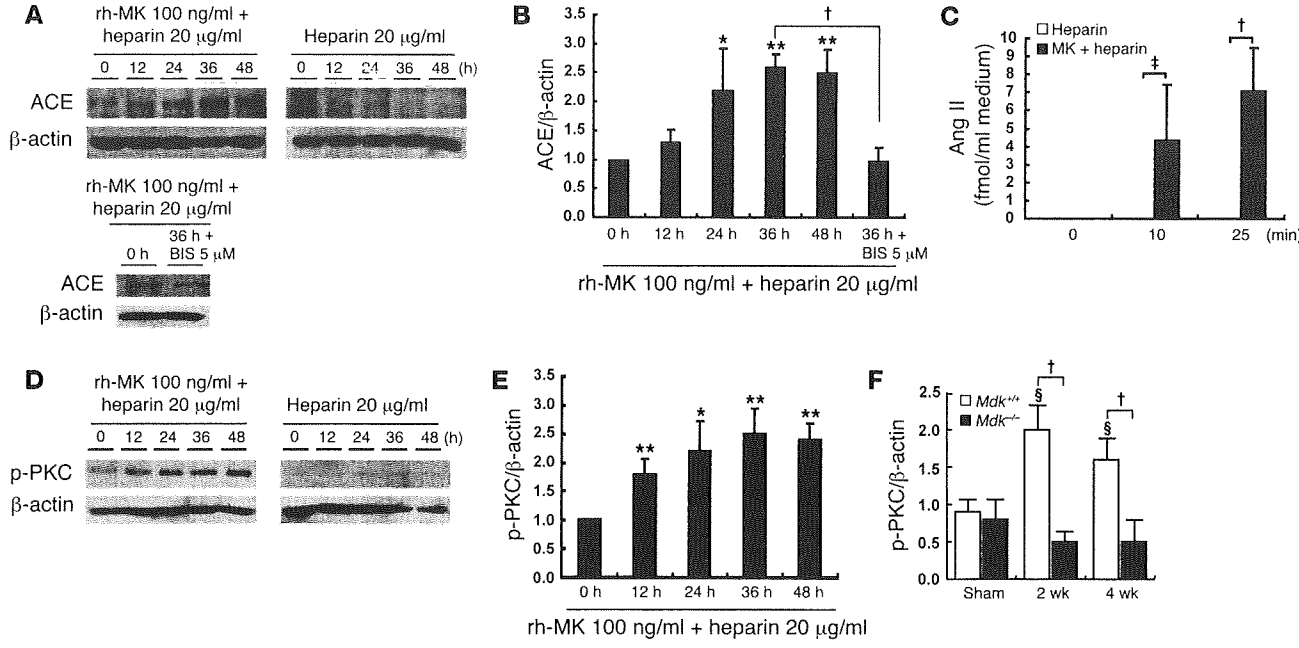

Figure 5
Mechanism of ACE induction by MK in HMVEC-L. (**A**) ACE expression in HMVEC-L treated with exogenous MK protein (100 ng/ml) and heparin (20 μg/ml). Lower panels: For PKC inhibition, BIS (5 μM) was added 1 hour before a 36-hour treatment with rh-MK plus heparin. Western blot data are shown. (**B**) The data in **A** were quantified using densitometry and are presented as mean and SD (n = 3). $^{*}P < 0.05$ and $^{**}P < 0.01$ versus 0 hours. (**C**) Conversion from Ang I to Ang II by the cells treated with MK. HMVEC-L cells were treated with exogenous MK protein (100 ng/ml) and heparin (20 μg/ml) or heparin (20 μg/ml) for 36 hours. Ang I (500 pM) was then added to the medium and incubated for the indicated times (n = 5). (**D**) Phospho-PKC expression in HMVEC-L treated with exogenous MK protein (100 ng/ml) and heparin (20 μg/ml). Western blot data are shown. (**E**) The data in **D** (left panel) were quantified using densitometry and are presented as mean and SD (n = 3). $^{*}P < 0.05$ and $^{**}P < 0.01$ versus 0 hours. (**F**) Representative data from Western blotting for phospho-PKC expression in the lung. The intensity of phospho-PKC bands on Western blotting was normalized to that of β-actin (n = 5). $^{\S}P < 0.05$ versus sham *Mdk*$^{+/+}$. Western blotting results are not shown. $^{\dagger}P < 0.01$; $^{\ddagger}P < 0.05$.

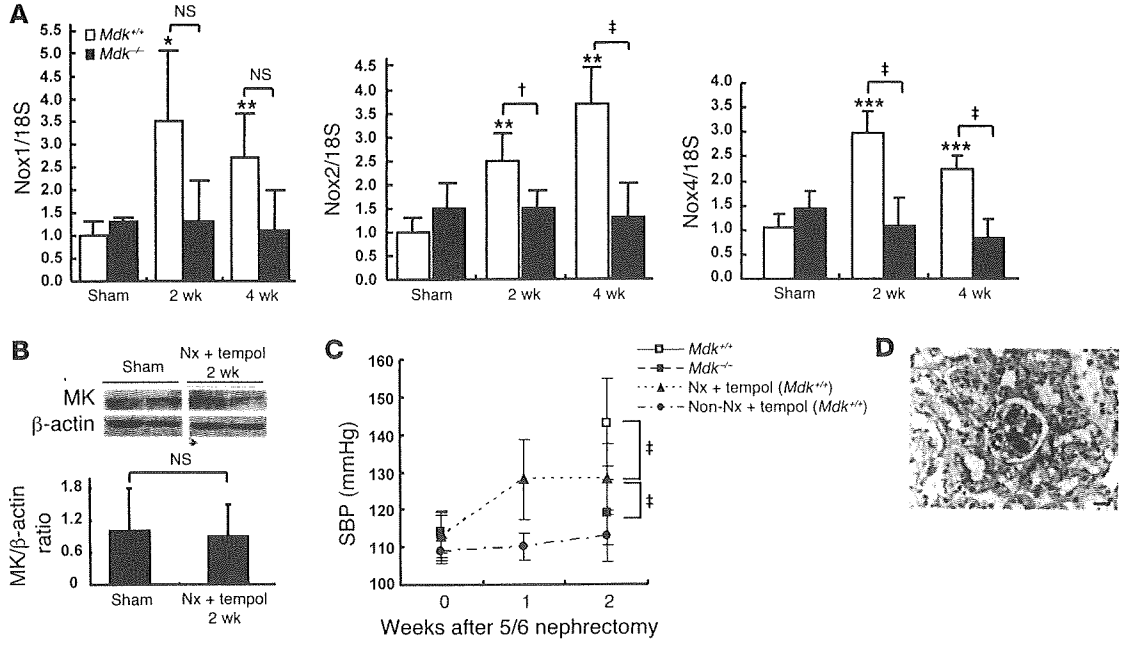

Figure 6

The mechanism of MK induction in the lung. (**A**) Time course of Nox1, -2, and -4 expression in the lung after 5/6 nephrectomy. Expression of Nox1, -2, and -4 mRNA was determined by real-time PCR. Data are presented as mean and SD (*Mdk*$^{+/+}$: sham, $n = 5$; 2 weeks, $n = 5$; 4 weeks, $n = 3$; *Mdk*$^{-/-}$: sham, $n = 3$; 2 weeks, $n = 3$; 4 weeks, $n = 3$). $^{*}P < 0.05$, $^{**}P < 0.01$, and $^{***}P < 0.001$ versus sham *Mdk*$^{+/+}$. (**B**) Effect of tempol on MK expression in the lung. Tempol mixed in drinking water was administered to *Mdk*$^{+/+}$ mice after 5/6 nephrectomy. MK protein expression was determined by Western blotting (upper panel). The intensity of MK bands on Western blotting was normalized to that of β-actin (lower panel). Data are presented as mean and SD ($n = 5$). (**C**) Effect of tempol on blood pressure after 5/6 nephrectomy. SBP was measured by the tail-cuff method. Data are presented as mean and SD ($n = 6$). (**D**) Effect of tempol on renal damage. PAS staining of a kidney specimen 2 weeks after 5/6 nephrectomy in *Mdk*$^{+/+}$ mice that received tempol treatment. The tubulointerstitial damage was slight compared with that in the mice without tempol treatment (Figure 1C). Scale bar: 20 μm. $^{\dagger}P < 0.05$; $^{\ddagger}P < 0.01$.

addition, we found a significant elevation of macrophage infiltration into the kidney in wild-type mice compared with *Mdk*$^{-/-}$ mice in the present study. This finding is consistent with our previous report showing MK-mediated macrophage recruitment in neointima formation (41). Therefore, MK-mediated inflammation in the kidney may contribute to the renal damage after 5/6 nephrectomy (Figure 7). On the other hand, in the context of inflammation and hypertension, it is important to note that inflammatory cell infiltration into the kidney does not always induce hypertension (42, 43). Furthermore, the local RAS in organs other than the lung was not activated in the present study. Thus, the relationship between intrarenal inflammation and hypertension after 5/6 nephrectomy remains to be verified.

Methods

Animals and experimental design. Mice deficient in *Mdk* were generated as described previously (44). After backcrossing of *Mdk*$^{+/-}$ mice for 14 generations with 129/Sv mice, *Mdk*$^{+/-}$ mice were mated with each other to generate *Mdk*$^{+/+}$ and *Mdk*$^{-/-}$ mice, which were used in this study. Experiments were performed on 8- to 12-week-old female mice weighing 20–25 g that were housed under controlled environmental conditions and maintained with standard food and water. Animal care and experimental procedures were approved by the Animal Experimentation Committee of the Nagoya University Graduate School of Medicine and were conducted according to the Nagoya University Regulations for Experiments. Renal ablation was performed as described previously. Briefly, mice were anesthetized by diethyl ether. The flank region was shaved, and the animals were placed on a heating pad to maintain a constant body temperature (37°C). Under anesthesia, right flank incisions were made, and the right kidney was removed. Seven days later, mice were anesthetized as above, and two-thirds of the mass of the left kidneys was ablated (*Mdk*$^{+/+}$: 2 weeks, $n = 13$; 4 weeks, $n = 13$; 8 weeks, $n = 8$; *Mdk*$^{-/-}$: 2 weeks, $n = 10$; 4 weeks, $n = 10$; 8 weeks, $n = 4$). After the renal ablation, the flanks were closed in 2 layers with 5-0 silk sutures. The animals received 100 ml/kg warm saline instilled into the peritoneal cavity during the procedure and were allowed to recover with free access to food and water. In the control mice, a sham operation was performed (*Mdk*$^{+/+}$, $n = 11$; *Mdk*$^{-/-}$, $n = 8$).

Drug treatment model. In the drug treatment studies, *Mdk*$^{+/+}$ mice were randomly assigned to receive one of the following 5 treatments after 5/6 nephrectomy and were orally treated daily starting from 24 hours after 5/6 nephrectomy: vasodilator (hydralazine hydrochloride; Novartis) at a dose of 10 mg/kg/d (group 1, $n = 3$); ACE inhibitor (temocapril; Daiichi Sankyo Co.) at a dose of 3 mg/kg/d (group 2, $n = 3$); angiotensin receptor blocker (olmesartan; Daiichi Sankyo Co.) at a dose of 3 mg/kg/d (group 3, $n = 3$); antioxidative reagent (tempol; Alexis Biochemicals) at a dose of 3 mmol/l in drinking solution after 5/6 nephrectomy (group 4, $n = 6$); and sham operation (group 5, $n = 6$). Drug treatment was performed at 2 weeks after 5/6 nephrectomy. In the present study, we determined the dosage according to previous reports (45–47). Blood pressure was measured by the tail-cuff method at 2 weeks, as described below under *Blood pressure monitoring*. Mice were sacrificed at 2 weeks after 5/6 nephrectomy, and blood and tissue samples were collected.